

RASCqL: Reaction-time-limited Architecture for Space-time-efficient Complex qLDPC Logic

Willers Yang*, Jason Chadwick, Mariesa H. Teo, Joshua Viszlai, Fred Chong

Department of Computer Science, University of Chicago

Chicago, IL, USA

Abstract

Quantum low-density parity-check (qLDPC) codes offer a promising route to scalable fault-tolerant quantum computing (FTQC) due to their substantially reduced footprint, but these gains can be diluted at utility scale if we cannot also realize a space-time-efficient instruction-set architecture (ISA) for relevant quantum applications. We present *RASCqL*, a Reaction-time-limited Architecture for Space-time-efficient Complex qLDPC Logic, introducing a complex-instruction-set quantum computer (CISQ) that supports key algorithmic subroutines such as quantum arithmetic, table lookups, and magic-state distillation directly in co-designed qLDPC codes.

Unlike prior constructions for qLDPC logic that aim at versatile ISAs amenable to diverse circuits, RASCqL adopts an application-tailored code-modification scheme that embeds specific complex Clifford instructions useful for functional subroutines as virtually implementable matrix automorphisms. RASCqL further leverages parallel physical operations in reconfigurable neutral-atom array platforms to achieve fast QEC cycles and high-fidelity transversal operations. At the cost of increased design complexity, RASCqL implements key algorithmic subroutines at space-time costs comparable to state-of-the-art transversal surface-code architectures while achieving up to 2 \times to 7 \times footprint reduction under realistic physical error rates of 2×10^{-3} – 5×10^{-4} , without additional hardware complexity. RASCqL thus demonstrates a concrete path forward for qLDPC codes as CISQ compute modules, extending their practical utility in fault-tolerant quantum computing architectures.

1 Introduction

Quantum computers promise polynomial complexity algorithms for many tasks currently without efficient classical solutions, including factoring [1] and chemistry simulations [2]. Implementing useful quantum algorithms requires a fault-tolerant quantum computer (FTQC) with logical qubits and operations achieving error rates as low as 10^{-9} to 10^{-16} [3], while current devices operate with physical error rates around 10^{-3} [4–6]. Quantum error-correcting codes (QECC) are deployed to bridge the gap between useful quantum advantage and noisy hardware, providing exponential error suppression when physical operations meet a code-specific

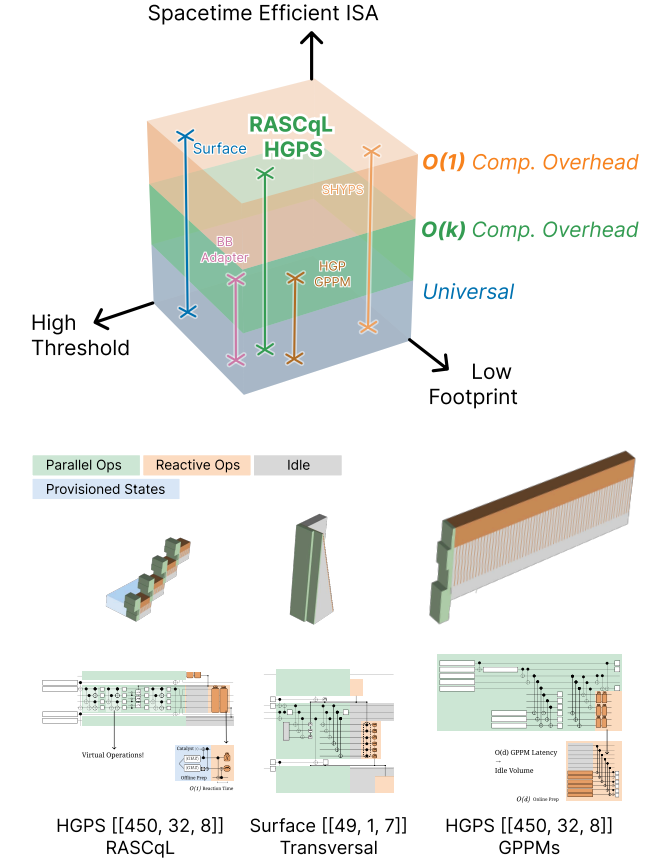


Figure 1. Top: RASCqL exhibits high circuit-level threshold, high encoding rate, and space-time efficient ISA for algorithms. Bottom: space-time volume comparison of RASCqL adder against baselines.

error threshold and defining a logical instruction-set architecture capable of universal quantum computation.

The *surface code* is a popular QECC due to its simple hardware requirements and expressive logical primitives, but suffers from overheads that scale polynomially in the number of correctable errors. Its syndrome extraction circuits require only 2D nearest-neighbor interactions, matching to planar superconducting devices with tunable couplers, and it tolerates physical error rates of around 1% [7], allowing experimental demonstrations of error suppression in existing devices [4]. Logical operations on surface codes form

*willers@uchicago.edu.

a compact, uniform instruction set, enabled by hardware-compatible lattice-surgery primitives for Pauli-based computation [8], or constant-time transversal gates on reconfigurable neutral-atom arrays (RNAA) with correlated decoding [9, 10]. These FT primitives, along with resource states prepared through distillation protocols [11, 12], can be composed efficiently to execute arbitrary quantum programs. Consequently, optimizing a surface code architecture often parallels RISC design: a standard, expressive ISA, heavily optimized across layers from algorithm mapping and resource estimation [3, 13–16] to logical-level compilation [17, 18] and hardware co-designs [19, 20]. The cost of simplicity, however, is that the surface code (as is the case with any codes with 2D-local checks) suffers from a qubit overhead that scales quadratically with the number of correctable errors, leading to resource estimations at $1000\times$ physical qubits to encode a single logical qubit [21].

Quantum low-density parity-check (qLDPC) codes, on the other hand, do not necessarily suffer from space-time overheads polynomial in d , at the cost of increased hardware complexity and limited instruction sets. Recently, studies on the algebraic structures of qLDPC codes have led to many hardware-efficient co-designs matching restricted code families to various physical architectures [22–24], turning them into promising alternatives to surface codes. When deployed as high-threshold, low-footprint quantum memories, such codes can expand the frontier of achievable quantum algorithms on qubit-constrained devices [25], potentially shortening the timeline for demonstrations of useful quantum advantage. Another disadvantage qLDPC codes face is access to efficient logical operations. At the asymptotic limit, there exists a fundamental trade-off between a qLDPC code’s memory performance and the efficiency of existing fault tolerant instructions [26], and in practice, ISAs of existing qLDPC codes are either limited in size and expressivity [22, 27], or require physical device capabilities beyond near-term devices [28].

While it appears challenging to realize utility scale general-purpose computation in qLDPC codes that simultaneously achieve high threshold, high rate, and space-time efficient ISA, these limits only hold if each block must independently support arbitrary circuits efficiently. Instead, we propose code constructions that possess limited but useful automorphism gates that, while not amenable to generic inputs, can directly accelerate common subroutines such as quantum adders, magic-state distillation, and quantum lookup. Unlike other proposals for logic in qLDPC codes that aim at a RISC ISA capable of handling arbitrary circuits, our perspective reframes in-block computation on qLDPC codes as a *Complex-Instruction-Set Quantum* (CISQ) architecture, where each code is co-designed to implement a limited, functionally-targeted set of logical operations natively and efficiently. For a visual example, Figure 1 shows how the quantum adders are compiled in RASCqL in comparison with other approaches.

A specialized logical ISA is particularly relevant for existing fault tolerant quantum workloads, where the space of useful applications is narrow with implementations dominated by few functional building blocks [10]. In particular, not only do they support factoring [21], adders also appear as the dominant cost in various chemistry applications [29–34]. As we will show, designing codes that excel at these common subroutines, rather than universally supporting arbitrary operations, is the key to efficient in-block computation with qLDPC codes.

We present *RASCqL*, a Reaction-limited Architecture for Space-time efficient Complex Quantum Logic, where we enable efficient and hardware compatible in-block computation in co-designed qLDPC codes with the potential to outperform surface codes. RASCqL makes three key contributions:

1. **Complex Quantum Logical Units (CQLU)** We design complex quantum logical units on co-designed qLDPC codes with useful complex quantum instructions and develop targeted SIMD compilations of key subroutines onto CQLU instructions. For adders, we achieve up to 7x footprint reduction with 1.25x Clifford-volume reduction against state-of-the-art transversal surface code baselines in a reaction-time limited compilation framework.
2. **Predictive Resource-state Preparation (PReP)** We predict resource state requirements for fast reactive operations and pipelined CQLU production. In particular, we achieve reactive Pauli Product measurements, arbitrary pattern CNOT fan-outs, and non-Clifford gates with $O(1)$ latency in expectation. Our optimized state factories achieve 10x volume reduction for $|GHZ\rangle$ states compared to surface code baselines, and demonstrate high fidelity magic states in LDPC codes with 2x footprint reduction and 3x increase in volume.
3. **Physical implementations on reconfigurable neutral atom arrays** We give explicit layout and AOD-compatible movement schedules to all primitives, achieving QEC cycles in millisecond scale, demonstrating subthreshold error suppression while carefully accounting for additional idle and gate error due to transversal logic, and produce realistic resource estimation for key subroutines used in factoring and chemistry simulations.

Together, these designs establish a CISQ framework and expand the practical utility of qLDPC codes beyond low-footprint memory. To our knowledge, RASCqL is the first to propose a class of hardware-compatible and high rate qLDPC codes that demonstrate quantum arithmetic modules with improved space-time volumes compared to state-of-the-art surface code baselines.

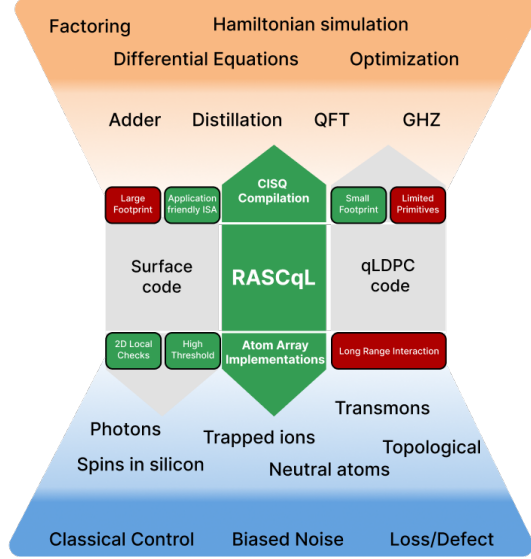


Figure 2. A three-stack view of FTQC. The surface code implements an efficient logical layer due to its hardware compatibility and RISC ISA, but suffers from large qubit overhead. qLDPC codes may reduce footprint, but require long-range interactions and have comparatively limited logical primitives. RASCqL achieves efficient in-block computation by co-designing qLDPC codes with CISQ compilations with key functional subroutines and reconfigurable neutral atom-array implementations.

The rest of the paper is organized as follows. We begin with an introduction to FTQC as a three layer stack in Section 2. Then, we describe RASCqL in Section 3. Code constructions, targeted compilations, resource state prediction, and physical RNAA implementations are described in Section 4, where detailed constructions and proofs are deferred to the Appendix. Finally, we compare the performance of RASCqL on subroutines including adders, GHZ and magic state preparation to state-of-the-art surface code baseline in Section 5, where explicit physical movement and gate schedules are used for resource estimation and a detailed circuit-level noise model is used for logical error rate simulations.

2 Background

A fault-tolerant quantum computer consists of a three-layer stack (Figure 2): the *functional layer*, where algorithms and subroutines are described by abstract quantum programs; the *logical layer*, where QECCs provide error suppression and fault-tolerant primitives that define the instruction set architecture (ISA); and the *physical layer*, where hardware parameters such as connectivity and noise model determine implementability, costs, and fidelity of QEC primitives. The logical layer forms a thin waist between applications and

diverse hardware, introducing a vast design space rich in optimization opportunities and potential inefficiencies.

2.1 Logical Layer: Quantum Error Correcting Codes

A quantum error correcting code (QECC)’s error suppression performance is summarized by four key parameters— n , k , d and p_{th} . A $[[n, k, d]]$ code encodes k logical qubits using n physical qubits, where a Pauli operator of minimum weight d is required to transform between logical states. p_{th} refers to the *error threshold*, or the physical error rate below which a code begins to work reliably. A QECC can correct up to $\lfloor \frac{d}{2} \rfloor$ errors below threshold by performing *syndrome extractions*, outcomes of which are used by a *decoder* to identify most-likely errors and compute corrections. In an error model where each physical Pauli error occurs independently with probability p_{phys} and assuming perfect syndrome extraction, the logical error rate (LER) can be exponentially suppressed according to the formula:

$$p_L \approx \left(\frac{p_{phys}}{p_{th}}\right)^{\lfloor \frac{d}{2} \rfloor + 1}. \quad (1)$$

While d and Equation 1 describe the theoretical capacity of a QECC, errors in realistic systems often deviate from idealistic assumptions. We can more accurately assess the LER performance of a code using circuit-level simulations that account for error propagation through syndrome extraction circuits and device-specific noise models.

The *encoding rate*, $\frac{k}{n}$, captures the code’s space efficiency; codes with lower rate will have larger per-logical qubit footprint on a device. Due to the parallelizability afforded by backwards-in-time gate teleportation [16], the space-time circuit volume is an important metric used to resource estimate quantum algorithms and evaluate FTQC system performance, in addition to LER. Current estimates place the circuit volume of realistic implementations of practical quantum algorithms such as factoring and chemistry simulation at millions of qubit-days [3], in part due to the large qubit-overhead associated with the leading proposal of using surface codes as the logic layer.

On the costs of error suppression is the increased difficulty in implementing an efficient, universal logical ISA. Indeed, a distance- d error protection also places the same restriction on the number of physical operations needed to effect logical transformation. In order to maintain fault tolerance, these logical operations must be implemented carefully to avoid propagating physical errors within the support of a logical qubit and reducing distance, while guaranteeing that additional errors from these physical operations are also detectable. Logical operations satisfying these conditions are said to be *transversal*. The existence and expressivity of transversal logical gates depend on inherent symmetries of the code in question, and no QECC can implement a universal set of logical operations transversally [35]. Consequently, an efficient logical ISA requires two components: an efficient

set of native fault-tolerant gadgets, usually a generating set of Clifford gates such as the CNOT, H, and S gates, or Pauli Product measurements, with a purification protocol to prepare non-native magic states to achieve universal computation [36]. In Figure 3, we summarize the key techniques for enabling fault-tolerant logical operations. The availability and costs of these gates further depend on the code and technique for logical operations.

2.1.1 The surface code. The *surface code*¹ is a $[[d^2, 1, d]]$ QECC with a threshold of about 1% under a fast matching decoder [7]. Analogous to the classical repetition code, it has a particularly simple construction—on a $D \times D$ grid of physical qubits, a surface code interleaves an equal number of X and Z checks that each covers four 2D-nearest-neighbor data qubits in a symmetric pattern, as illustrated in Figure 3. As is the case for all QECCs with local checks, the surface code suffers from a qubit overhead that scales quadratically with distance.

There are two approaches for logical operations on surface codes. On fixed-topology hardware such as superconducting qubits, we can perform arbitrary multi-qubit Pauli-product measurements (PPM) using lattice surgery with an additional $O(d)$ time overhead, leading to an overall space-time volume of $O(d^3)$ qubit-cycles for each instruction [18]. In addition, CNOT, S, and H gates can be performed transversally on RNAAs with $O(1)$ time overhead using correlated decoding [9], reducing the space-time overhead to $O(d^2)$ per instruction.

2.1.2 qLDPC codes. A QECC is said to be low-density parity-check if the number of other physical qubits each qubit interacts with is upper bounded during an error correction cycle. This LDPC condition limits how far a physical error can propagate, and is necessary to ensure fault-tolerance. While the surface code is also a qLDPC code, general constructions do not impose locality constraints that lead to undesirable overheads. The first constant rate qLDPC code discovered uses good classical LDPC codes as seeds in a Hypergraph-Product (HGP) construction [38]. More recently, high rate qLDPC codes with concrete physical implementations have also been discovered that exhibit exponential error suppression under realistic physical error rates [22, 23].

While proposals for qLDPC in-block computation exist, they are often much more difficult to compile to or implement on hardware. The leading proposal realizes the lattice-surgery style RISC as universal adapters, although current designs prioritize small footprint adapters with favorable planar embedding but limited native operations, leading to additional spacetime volume caused by long gate decompositions that eclipse the space savings in practice [39]. Another less versatile proposal uses code automorphism—*intrinsic*

¹We focus on the rotated surface code [37], which achieves a higher encoding rate and threshold among variants.

symmetries of the QECC—that in rare cases allow complex logical operations to be implemented transversally. However, stringent conditions need to be met to lift these symmetries to fault tolerant logical operations [40], and they often manifest as arbitrary global transformations that do not find direct applications easily [27]. Automorphism gates in performant qLDPC codes often serve to implement memory operations such as qubit permutations [25, 39, 41].

2.1.3 Magic State Distillation. A key limitation to QECC is the aforementioned lack of universal native instructions. A standard approach is to supplement the logical ISA with high fidelity resource states that can implement non-native operations fault tolerantly. These states can be prepared using a magic state distillation (MSD) protocol, where fault-tolerant Clifford operations are used to purify noisy magic states. For example, the $[[15, 1, 3]]$ protocol outputs a $|T\rangle$ state at error rate $O(p^3)$ with high probability, using 15 noisy $|T\rangle$ states at physical error rate $O(p)$. These magic states can then be used to synthesize universal gates with $O(\log \frac{1}{\epsilon})$ overhead to a target error rate ϵ [42]. Due to its high overhead, it is estimated that as high as 95% of computing volume may be spent on producing high-fidelity magic states [43], making it an important bottleneck to FTQC. In this work, we will focus on a family of MSDs described by Hastings and Haah [11] which includes the $[[15, 1, 3]]$ codes to limit scope, though our methodology extends to Reed-Muller codes and triorthogonal codes more generally.

2.2 Physical Layer: Reconfigurable Atom Arrays

qLDPC codes and transversal logic require high-fidelity non-local interactions. One approach is to use platforms that support programmable qubit movement, implementing flexible connectivity through physical reconfiguration, such as RNAAs where neutral atom qubits can be moved in parallel using optical tweezers [6]. Several other proposals exist to realize these requirements in hardware, including modular architectures with photonic interconnects [16, 44], all-to-all connected trapped-ion qubits with long-range Coulomb-mediated gates [45], and superconducting architectures with a few interconnected layers of planar tunable couplers [22]. While these approaches provide pathways to long-range connectivity, current experimental demonstrations are limited in scale—typically in the range of a few to a few dozen qubits [5, 44–46]—well below requirements for utility-scale FTQC. On the other hand, up to 6100 qubits have been demonstrated on neutral atom processors [47]. For this reason, we will focus on RNAAs in our designs and analysis.

Neutral atom arrays have been demonstrated to have seconds-long coherence times, with high fidelity single- and two-qubit gates [6, 47, 48]. An RNAA device is bottlenecked by movement and measurements—while physical operations only take on the order of micro-seconds, atom motion and

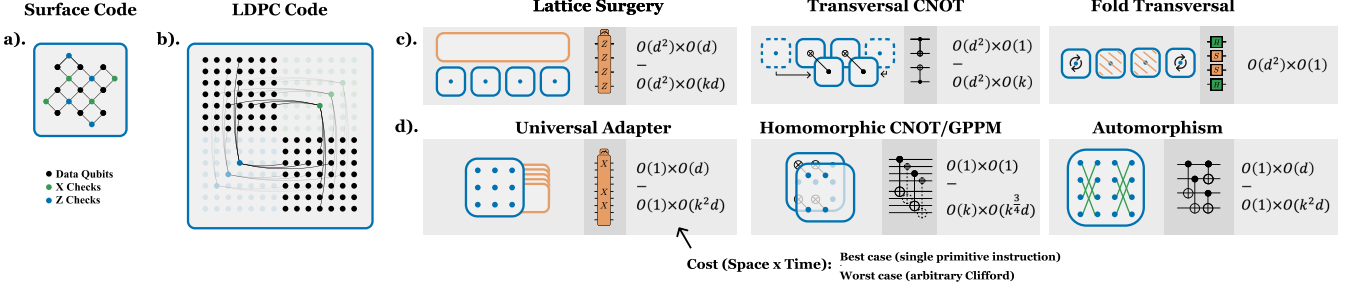


Figure 3. Quantum error correcting codes. a) $[[9, 1, 3]]$ surface codes with 2D planar syndrome checks. b) $[[98, 18, 4]]$ qLDPC code with non-local syndrome checks and improved encoding rate. c) Fault tolerant logical instructions of a surface code: (from left to right) arbitrary Pauli Product measurements, parallel transversal CNOTs, and addressable single qubit Clifford gates. d) Fault tolerant logical instructions of qLDPC codes: particular Pauli Product measurements given by a universal adapter, global transversal CNOTs, and automorphism Clifford gates given by code symmetries.

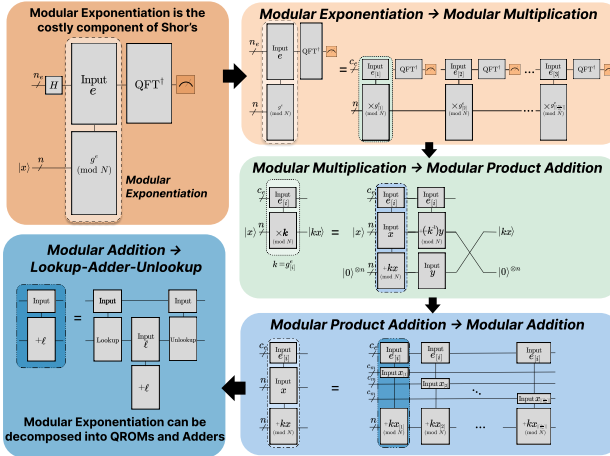


Figure 4. Abstract overview of the factoring algorithm. It can be implemented using repeated applications of quantum adders and quantum look-up tables, with a QFT.

measurement can take orders of magnitude longer, requiring up to half a millisecond [10]. One prevalent architecture model for neutral atoms is the zone-based architecture, which separates space into storage zones, entangling zones, and readout zones, into which qubits have to be moved to undergo zone-specific operations [6]. This architecture requires motion before every entangling gate and measurement, which can become a limiting factor in computation. Instead, we focus here on an architecture combining motion with free-space measurement, as is done in the baseline work we compare to [10], and use the same set of hardware parameters for a fair comparison. The logical operation of such an architecture has been demonstrated at a small-scale, with parallelized qubit control and acceleration-based movement (the duration of motion scales as a square root of the distance moved) [48, 49].

2.3 Functional Layer: Quantum Algorithms

Developing quantum algorithms with a speedup over classical methods has been an active area of research since the emergence of quantum computing, resulting in algorithms for integer factoring [1], search and optimization [50], combinatorial optimization [51, 52], quantum chemistry [29–34, 53], and more [54–56]. Here, we introduce two prominent examples of FTQC applications, factoring and quantum chemistry, which feature common subroutines our CISQ architecture can be optimized for.

2.3.1 Factoring. Shor’s algorithm solves the integer factoring problem – given N , the aim is to find factors p and q such that $N = p \times q$. The algorithm is a hybrid classical-quantum algorithm whose quantum component focuses on period-finding, or in other words, for some a , finding the smallest r such $a^r \equiv 1 \pmod{N}$. Period-finding can be broken down into a modular exponentiation, followed by a quantum Fourier transform. As the modular exponentiation dominates the cost of period-finding, many resource estimates focus on this part of the algorithm [10, 13, 21], which can be implemented using windowed arithmetic that decomposes into sequences of adder and quantum read-only memory (QROM) subroutines [57] (see Figure 4).

2.3.2 Quantum Chemistry. These subroutines are also useful in quantum chemistry applications which use qubitization and quantum walk-based methods. Among other chemistry applications that utilize quantum arithmetic [29–34, 53], one salient application is determining the ground states and ground state energy of a given Hamiltonian [53, 58, 59]. These algorithms use PREPARE and SELECT oracles to encode a Hamiltonian, where PREPARE blocks perform state preparation of a superposition state and SELECT blocks implement the ℓ th term in the Hamiltonian on the target register if the ancilla register is in the state $|\ell\rangle$ [15, 34, 58]. These oracles, in turn, are largely composed of adder and QROM

subroutines, making them crucial complex instructions for an efficient FTQC.

The utility of adders and QROM extends beyond factoring and quantum chemistry: the adder subroutine is used more generally to implement quantum arithmetic, n single-qubit rotations, and the n -qubit phase gradient operation [60]; QROMs are key components of protocols for state preparation and unitary synthesis [61]. Building on the insight that several state-of-the-art quantum algorithms decompose into a finite set of common functional subroutines, the performance of a logical architecture can largely be captured by how efficiently it can implement a select number of subroutines. The decomposition of large-scale algorithms into core subroutines points to a scalable CISQ strategy that leverages the efficient operations unique to specific qLDPC codes.

We note that while we focus in this paper on construction and resource estimates for the adder, the methods we describe, such as the implementation of CNOT- fanouts and Toffoli ladders, extend to QROMs as well.

2.4 Full Stack Fault-Tolerant Quantum Architectures

Resource costs for FTQC have continuously improved over the past decade due to improving encoding rates and more efficient techniques for logical action. More recently, ISA (co-)design and memory hierarchy proposals have unlocked additional gains from the system level.

Initial proposals for an FTQC relied on multiple layers of concatenated codes such as Steane codes [62]. These schemes provided a clear theoretical foundation, but their resource costs scale exponentially to the number of correctable errors. On the other hand, surface code architectures promised only quadratic qubit overhead. Logical computation on surface codes has evolved substantially: early proposals relied on defect braiding [7], while later approaches introduced lattice surgery for more space-time-efficient merge-split operations [18]. Recently, symmetry-based constructions enabling transversal logical operations have further reduced overhead in tailored architectures [63]. The state of the art (SoTA) architecture proposal on reconfigurable atom arrays uses surface codes with transversal decoding, which we use as a baseline for comparison [10].

qLDPC codes can potentially achieve 10x qubit-reduction with near-term devices, while at present they often struggle to implement algorithms due to the lack of generically applicable logical ISA. One way around this is to use qLDPC as low-footprint quantum memory in a hierarchical system, where surface codes are still used for logical computations [21–25]. While achieving a reduction in footprint, such systems may be bottle-necked by I/O for applications with high parallelism[24, 25], and may be less efficient from the space-time cost perspective. With various methods to trade between space and timecosts[64], compilations of practical algorithms that targets space-time volume can avoid inherent program-serializations to more effectively mitigate the

impact of high idle volumes [16], which may limit the range for memory hierarchy proposals to find substantial application.

While there exist certain efficient logical operations that are more space-time efficient in qLDPC codes [41, 65], it remains challenging to show competitive space-time performance at utility scale for generic quantum algorithms due mismatched priorities across the stack. The dense packing of logical qubits also allows certain complex Clifford operations arising from symmetries of the code to be implemented transversely in batches at low to no cost [28, 66], whereas a baseline surface code may often resort to an $O(kd^3)$ -volume lattice-surgery sequence. However, such operations may not directly find applications for generic circuits, which are often expressed with a surface-code inspired RISC instruction set. Attempts to recreate such RISC ISAs on qLDPC codes either require capabilities beyond intermediate-term devices, or restrict to hardware-compatible designs that are often space-time inefficient. For example, the Subsystem Hypergraph Simplex (SHYPS) codes can implement generic Clifford operations with constant space-time overhead, while its stabilizers have weights that scale with code length, requiring orders of magnitude more strict requirements for physical error rates at high distances. On the other hand, IBM’s Bivariate Bicycle (BB) codes with universal adapters [39] prioritize hardware compatibility where both LDPC and bi-planarity properties are maintained and have high threshold, but comes with a limited ISA that leads to long gate decomposition sequences when compiling for practical algorithms.

RASCqL takes the natural next step in the evolution of quantum architectures by viewing qLDPC codes as specialized accelerators for complex instructions, and shows that overall space-time reduction is attainable, even with realistic error rates for practical algorithms. We pay the cost in terms of flexibility and increased design complexity, which we argue is a worthwhile trade-off for existing quantum workloads that require few key subroutines. Unlike memory hierarchy proposals, RASCqL implements all logical operations in-block in a reaction-time limited framework, avoiding costly inter-code communication, while retaining footprint advantage. RASCqL targets a practical class of algorithms such as factoring and chemistry simulations, and unlike codes designed to be efficient for generic inputs such as *SHYPS*, RASCqL remains LDPC, with a circuit-level threshold of around 0.78%. RASCqL is also hardware-compatible, with structures that match RNAA capabilities. Compared to other hardware efficient approaches, while RASCqL’s ISA is not necessarily more expressive, they are co-designed to contain complex instructions that are efficient for applications, accompanied with reaction-time limited compilations of specific key subroutines that are sufficient for the majority of factoring and chemistry simulations.

3 RASCqL Architecture

In this section, we describe RASCqL, a complex instruction set quantum (CISQ) computer architecture in qLDPC codes. First, an input quantum algorithm is compiled using a set of supported algorithmic subroutines. Two main subsystems enable efficient execution of these subroutines as complex instructions on qLDPC codes: 1). a suite of co-designed Complex Quantum Logic Units (CQLU) that realizes a limited but useful ISA in-block, and a tailored compilation of subroutines using this ISA; and 2). a Predictive Resource-State Preparation (PReP) protocol that allows efficient generation and low-latency consumption of resource states for non-native and reaction-time limited operations. Finally, CQLU and PReP primitives are implemented using parallel AOD movement and Rydberg interactions on RNAA architectures, which allows us to obtain RNAA-realistic logical error rate simulations and resource estimations. See Figure 5 for an abstract overview.

3.1 CQLU Design

First, we identify an ISA consisting of few low-order Clifford operations that a) is efficiently supported on some qLDPC codes and b) efficiently supports all desired subroutines. Starting with generic codes and applications, we propose LDPC-preserving code modifications that allow us to embed a prescribed group of logical Clifford gates as code automorphisms of an arbitrary qLDPC code, as we will show in Section 4.1. This code modification introduces additional footprint in general that scales with both the size of the ISA and available symmetry of the starting code that should be co-optimized for given applications. Our ISA design, detailed in Section 4.2, co-optimizes compilation and code construction to target magic state distillation, factoring, and certain chemistry simulation tasks. Our lightweight ISA with few complex entangling instructions is sufficient, except for gates that vary with problem instance, such as reactive measurements or the CNOT fan-outs in quantum lookup, as we will show in Section 4.3. These instance-specific gates are implemented using gate teleportation, which requires $O(1)$ reaction time with provisioned resource states. We choose a family of Hypergraph Product of Simplex (HGPS) codes as the starting code, whose available primitive instructions already contain useful automorphisms such as dirty permutations and certain CNOT operators that support this ISA with minimal overhead. We further highlight the $[[450, 32, 8]]$ codes that require no overhead at all for this ISA.

3.2 PReP Design

Resource states serve two purposes in RASCqL. Firstly, magic states and stabilizer states such as $|T\rangle$, $|i\rangle$ and $|GHZ\rangle$ support non-native gates including T gates and instance-specific CNOT fan-outs. The consumption schedule of these states is deterministic and may be prepared offline. Secondly, logical

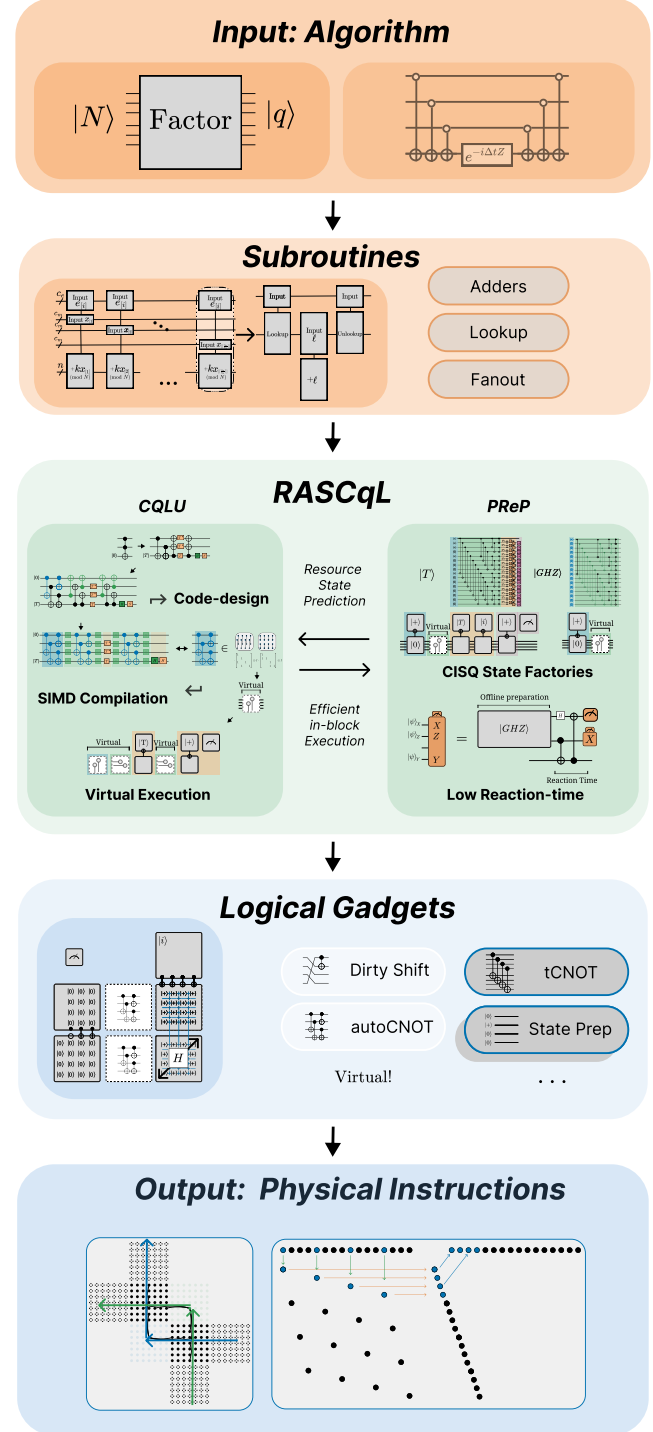


Figure 5. RASCqL Overview. Input algorithms supported by key subroutines are implemented using Complex Quantum Logic Units (CQLU) in tailored qLDPC codes and Predictive Resource-state Preparation (PReP) optimized using CQLU complex instructions. Logical primitives are then compiled down to parallel physical instructions on reconfigurable neutral atom arrays to obtain realistic estimations for logical performance and space-time cost.

ancillae are used for *reactive measurements*—addressable measurements in a basis that may depend on previous measurement outcomes—arising possibly from magic state injection or parallelization. The speed at which we can implement reactive measurements determines the program runtime and overall volume in the *reaction-time limited* compilation framework, which is the current SoTA for algorithms such as factoring.

PReP decouples state production from program execution using prediction and catalysts, reducing reaction time to $O(1)$ in expectation and unlocking additional resource savings from pipelining. First, PReP predictively provisions a pool of modified $|GHZ\rangle$ states that can implement reactive measurements in $O(1)$ time [67]. As we will show in Section 4.5.1, only a single type of states needs to be prepared if we allow additional constant time CQLU operations on the fly. PReP also maintains a generating set of $|i\rangle$ states on diagonal locations that serve as catalysts to perform arbitrary patterns of X/Y -basis reactive measurements which arise in MSD circuits. Finally, all resource states are generated in qLDPC blocks with optimized CQLU protocols, unlocking additional gains from high-rate magic state distillation and pipelined state production protocols.

3.3 RNAA Implementation

RASCQL is also equipped with a physical compiler to implement QEC primitives efficiently on an RNAA device. Memory cycles and complex instructions on CQLUs are compiled to explicit AOD movements, gate schedules, and mapping, which determines the real-time costs of each logical instruction. RASCQL’s physical scheduler uses fast and parallel systolic movements to achieve complex qubit permutations and memory cycle times on a millisecond scale, exploiting the algebraic structure of the codes and transversal logic. Details are given in Section 4.4. A simple greedy mapper is employed to minimize interaction distance, which can also be adapted for a zoned architecture.

Furthermore, an accurate circuit level noise model is used to assess the logical error rate performance of the proposed code that factors in additional gate errors and idle time due to transversal logic. For a neutral atom implementation of HGPS codes, we observe a high circuit level threshold of 0.78%, as shown in Section 5.1. We use the fits obtained from these simulations to estimate system-level costs of logical subroutines.

4 Methods

4.1 CQLU Construction

Given an error correcting code, it is well understood how to determine the set of logical operators arising from its code automorphisms[27, 40]. However, given an efficient ISA for a class of applications, the question of how we can construct a QECC containing specific logical operations is both less

explored and more practical to consider. Our CQLU design makes two technical contributions to the latter question: first, we adapt code modification techniques such as augmentation and extension for the purpose of embedding a logical operation as matrix automorphisms; secondly, we identify a class of highly symmetric HGPS codes that require little modifications to achieve an efficient ISA. We summarize the codes and logical ISA in Table 1, Table 2 and Figure 6 while detailed proofs are deferred to Appendix 7.

We will introduce a motivating example. Formally, given a binary linear code C with generator matrix G and parity check matrix H , an automorphism on C refers to a coordinate permutation σ that preserves the space of all code words. That is, there exists some invertible linear transformation g , such that

$$gG\sigma = G. \quad (2)$$

Equation 2 is called the *automorphism condition*. To enact the induced logical action of g on the classical code C , one can virtually permute coordinates, and modify subsequent encoding/decoding. When using C to construct a quantum code such as the Hypergraph Product code, a stricter condition of *matrix automorphism* is necessary for automorphisms (g, σ) to realize a permutation-transversal logical operation[40], where

$$H\sigma = \rho H \quad (3)$$

for some row permutations ρ . When σ is a matrix automorphism for some classical code C , the induced logical action lifts to a fault-tolerant logical operations $g \otimes I$, $I \otimes g$, or $g \otimes g$ on the HGP of C , all of which are implementable as virtual qubit-relabeling.

We do not expect codes to contain non-trivial automorphisms in general. For example, consider the smallest binary error correcting code with two logical bits—a $[5, 2, 3]$ shortened Hamming code—with generator and check matrices:

$$G = \begin{bmatrix} 1 & 1 & 1 \\ 1 & 1 & 1 \end{bmatrix}, \quad (4)$$

$$H = \begin{bmatrix} 1 & 1 & 1 \\ 1 & 1 & 1 \\ 1 & 1 & 1 \end{bmatrix}. \quad (5)$$

The SWAP between the two logical qubits is an automorphism-induced gate of G . By physically swapping the first two physical bits, and then the third and fifth bits, we obtain a new basis G_{SWAP} that corresponds to swapping the two rows of G . However, performing a CNOT between the two encoded bits (which corresponds to applying $g = \begin{bmatrix} 1 & 1 \\ 1 & 1 \end{bmatrix}$), would yield

$$gG = \begin{bmatrix} 1 & 1 & 1 \\ 1 & 1 & 1 \end{bmatrix} \quad (6)$$

that clearly cannot be obtained from G via a column permutation since it contains a weight-4 row.

Suppose we are given a logical action g and a code G , can we obtain a related code G' that implements g as a coordinate permutation? In this case, it suffices to add a single column $\begin{bmatrix} 1 \\ 1 \end{bmatrix}$, which yields

$$gG' = \begin{bmatrix} 1 & 1 \\ 1 & 1 \end{bmatrix} \cdot \begin{bmatrix} 1 & 1 & 1 & 1 \\ & 1 & 1 & 1 \end{bmatrix} \quad (7)$$

$$= \begin{bmatrix} 1 & 1 & 1 & 1 \\ 1 & 1 & 1 & 1 \end{bmatrix} \quad (8)$$

$$= G' \cdot \sigma_P \quad (9)$$

where σ_P is a column permutation that swaps the first three columns with the last three columns. That is, an augmentation on G yields a $[6, 2, 4]$ code G' whose automorphism group is expanded to include an additional logical gadget g .

We can prove a loose upper-bound for a generic code:

Theorem 1 (Code Automorphism Expansion). *Let us be given a $[n, k, d]$ code $C(G, H)$ and $\mathcal{G} = \{g_1, \dots, g_m\} \leq \text{GL}_k(\mathbb{F}_2)$. There exists a family of $[n' \leq nm, k, d' \leq dm]$ codes $C_{\mathcal{G}}(G_{\mathcal{G}}, H_{\mathcal{G}})$ such that $C \cong C_{\mathcal{G}}$, $\mathcal{G} \leq \mathcal{L}_{G_{\mathcal{G}}}(C_{\mathcal{G}})$. Furthermore, if H is w -bounded, g is t -bounded for all $g \in \mathcal{G}$ and $|\mathcal{G}| = m$, there exists a $(w + t + 1)$ -bounded check matrix $H_{\mathcal{G}}^{(t)}$ and a $(w + m + 1)$ -bounded check matrix $H_{\mathcal{G}}^{(m)}$.*

Theorem 2 (qLDPC with Virtual Instruction). *Let us be given $C(G, H)$ and $\mathcal{G} \leq \text{GL}_k(\mathbb{F}_2)$. Suppose H is w -bounded, g is t -bounded for all $g \in \mathcal{G}$ and $|\mathcal{G}| = m$. Then, there exists a family of $[[nm, k, dm]]$ codes $C_{\mathcal{G}}(G_{\mathcal{G}}, H_{\mathcal{G}})$ with a $2(w + mt + 1)$ -bounded check matrix $H_{\mathcal{G}}$ such that $g \in \mathcal{G}$ can be implemented as a virtual qubit relabeling.*

The detailed proof is given in Appendix 7, which also includes some useful scenarios of when such code modifications incur low overheads.

4.2 CQLU Logical Primitives

While our code modification techniques apply generally to all codes, its performance and whether we have the LDPC guarantee depend on the ISA we wish to embed and the starting classical code, which should be co-optimized with a chosen application.

In this work, we highlight a family of hypergraph product (HGP) codes, Q_r , with classical Simplex codes S_r as seed codes. Since the classical simplex code contains all reversible linear operations as code automorphisms[28], no additional overhead is required for automorphism expansion. There also exists a weight-3 circulant parity check matrix (pcm) that contains a set of logical cyclic shifts with additional CNOTs from the qubit shifted (see Figure 6.b) as matrix automorphisms. We call these shifts dirty cyclic shifts. In an HGP construction, these matrix automorphisms can either be used to perform CNOTs between specific qubits in fixed

Codes $([[n, k, d]])$	Footprint $(\frac{n+m}{k})$	Cycle Time
$[[450, 32, 8]]$	29.2 \times	3.9 ms
$[[90, 8, 10(\leq 8)]]$	22.5 \times	6.5 ms
$[[49, 1, 7]]$	98 \times	1.4 ms
$[[81, 1, 9]]$	162 \times	1.4 ms

Table 1. Comparison of space- and time-overheads of Q_4 , a Hypergraph-Product of Simplex code with the rotated surface codes [43] and bivariate bicycle codes [22]. Cycle times are calculated using systolic scheduling [24] on a RNAA device. The improved cycle time is due to Q_4 having a simple cycle structure, where X/Z checks are only shifted in one direction, as opposed to two—which is the case for the $[[90, 8, 10(\leq 8)]]$ bivariate bicycle code.

positions, or a cyclic shift provided that either the control qubit is set to $|0\rangle$ or the target qubit is set to $|+\rangle$.

Additionally, a 4-bit CNOT circuit g_{auto} (see Figure 6.a) is embedded as a matrix automorphism. Since $g_{auto}^2 = I$, the check extension incurs at most $2\times$ overhead. In particular, for the $[[450, 32, 8]]$ code Q_4 , there exists a pcm that contains both the dirty shifts and g_{auto} as matrix automorphisms with no additional overhead. g_{auto} lifts to 16 qubit CNOT circuits in an HGP construction that correspond to $g_{auto} \otimes I$, g_{auto} applied to each column; $I \otimes g_{auto}$, g_{auto} applied to each row; or $g_{auto} \otimes g_{auto}$, as illustrated in Figure 6.a. The full ISA is summarized in Figure 6 and Table 2.

4.3 Logical-Functional Compilation

4.3.1 State Preparation Circuits. We can use g_{auto} to prepare a GHZ state on all qubits in the same block, as illustrated in Figure 7. We can grow the GHZ state across multiple patches using transversal CNOTs between a $|GHZ\rangle$ patch and $|0\rangle^{\otimes k}$ patches. To prepare a GHZ state with arbitrary support, we can first entangle all qubits, and then selectively measure out qubits not in the support by preparing a mixed $|0\rangle / |+\rangle$ state in the corresponding pattern.

For MSD circuits, the only non-native operation required is the magic state injection, as illustrated in Figure 7, which dominates resource costs. We expect that as better schemes are developed for magic state injection, RASCqL’s performance may improve in tandem.

4.3.2 Quantum Arithmetic. We use Gidney’s ripple carry adder that uses $4n + O(1)$ T gates for an n -bit adder[68], where each MAJ and UMA block is compiled using time optimal methods [64]. We then re-write this circuit so the bulk of the Clifford gates can be executed in the CQLU ISA. In particular, the 3-bit fan-outs and fan-ins within the MAJ block are realized using repeated applications of g_{auto} and global H , while the Bell-preparation and Bell-measurement can be realized using tCNOTs by storing the bridge qubits in a separate qLDPC block. The Pauli corrections from Bell-measurements and Clifford corrections from $|T\rangle$ injections

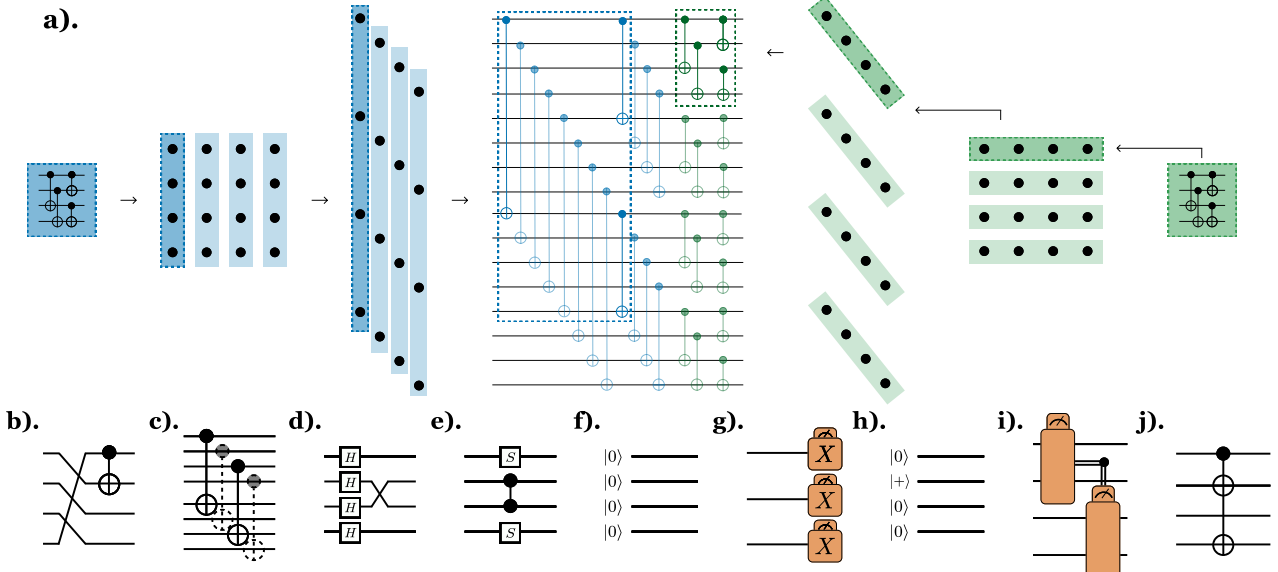


Figure 6. Set of logical instructions on CQLUs

Instructions	Total Time	Logical	Ancilla	Reaction Time	Execution Time
a). Automorphism CNOTs (autoCNOTs)	0	0	0	0	0
b). Dirty Cyclic Shifts	0	0	0	0	0
c). Transversal CNOTs (tCNOTs)	$O(1)$	0	0	$O(1)$	3.0 ms (+2.4 ms)
d). H -SWAP	$O(1)$	0	0	$O(1)$	1.9 ms
e). CZ - S	$O(1)$	0	0	$O(1)$	1.9 ms
f). $X^{\otimes k}/Z^{\otimes k}$ Measurements	$O(1)$	0	0	$O(1)$	0.5 ms
g). $ 0\rangle^{\otimes k}, +\rangle^{\otimes k}$	$O(d)$	0	0	$O(1)$	0 (31.2 ms)
h). Mixed $ 0\rangle, +\rangle$ States	$O(d + \sqrt{k})$	$O(\sqrt{k})$	0	$O(1)$	6.0 ms (+31.7 ms)
i). Reactive PPM	$O(d + \sqrt{k})$	$O(\sqrt{k})$	0	$O(1)$	6.0 ms (+44.2 ms)
j). Arbitrary Fanouts	$O(d + \sqrt{k})$	$O(\sqrt{k})$	0	$O(1)$	6.0 ms (+38.2 ms)

Table 2. CQLU ISA and costs. Gates a). and b). can be implemented virtually via qubit relabeling, which may incur additional 2.4 ms execution time for the next tCNOT. For gates g).–i)., we assume an logical ancilla is prepared offline. The total execution time without provisioning is reported in parentheses.

are propagated past the Z -basis measurements, turning them into reactive measurements with basis depending on previous measurement results. In the end, all operations in the gray box are executed in parallel using cheap in-block operations, followed by reactive measurements that are resolved in series with $O(1)$ delay.

The quantum look-up tables can be implemented by combining Toffoli ladders (which appear as a subcircuit of the MAJ block) and CNOT-fanouts (which can be implemented by injecting a GHZ state).

4.4 Logical-Physical Compilation

In this section, we describe our hardware assumptions, and how we achieve realistic estimates for the time costs of CQLU primitives. We also describe explicit layouts and schedules to

implement non-trivial permutations exploiting the parallel atom re-arrangements in RNAA platforms.

4.4.1 Hardware Assumptions. For our estimates we presume a RNAA device that supports both mid-circuit, parallel atom movement via AODs and in-place measurement of ancilla qubits. High fidelity atom movement has been demonstrated in experiment [6], leading us to assume moving distance l requires time $2\sqrt{l/a}$ for an acceleration of $a = 5500 \text{ m/s}^2$, consistent with prior work on QEC architectures in RNAA [10]. In-place measurement of ancilla qubits has also been demonstrated in experiment in dual-species [69] neutral atom devices. We note that RASCQL is not reliant on in-place measurement and is also compatible with a zoned architecture [6] where ancilla qubits are moved to a separate zone for measurement.

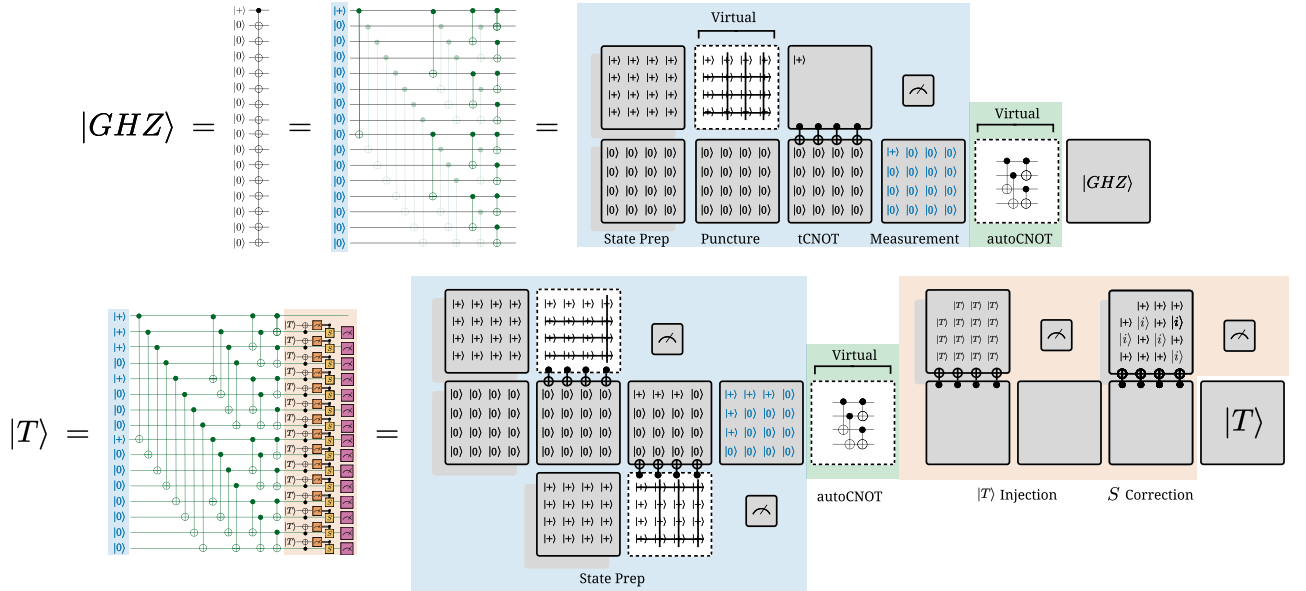


Figure 7. State preparation circuits using CQLU instructions. The initial Pauli eigenstate state preparation (highlighted in blue) can be done by preparing two (in the case of GHZ) or three (in the case of $[15, 1, 3]$) patches in X or Z eigenstates followed by puncturing and homomorphic measurements[41]. The entangling operations (highlighted in green) can be done using virtual embedded CNOTs, where the shaded CNOTs in the GHZ circuit act trivially. Magic state injection (highlighted in gray) is performed using a non-native universal adapter scheme. The Clifford correction (highlighted in orange) is implemented as a mixed X/Y reactive measurement.

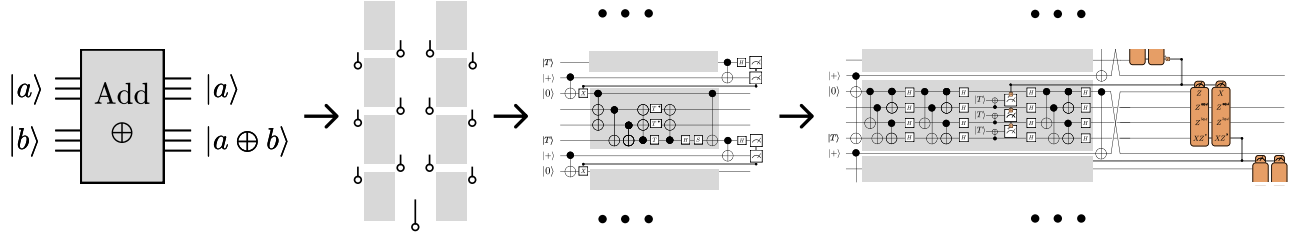


Figure 8. Gidney’s ripple carry adder[68] compiled using CQLU instructions. Eight MAJs can be implemented in each block with the same time cost. See Appendix D for a detailed derivation.

4.4.2 Syndrome Extraction. The qLDPC codes described in this work are HGPs of the classical Simplex codes, which are themselves constructed from cyclic permutation matrices. The codes are therefore closely related to Generalized-Bicycle codes and benefit from the same movement parallelism exploited in [24]. Based on this insight we create an efficient movement schedule for reconfigurable neutral atom devices detailed in Figure 9. Since all CNOT orderings for HGP codes are distance-preserving [70], our schedule uses an ordering that minimizes the required movement. To improve movement times, we break the schedule into alternating rounds. Importantly, in each schedule the X stabilizers (green) interact with each data qubit first, ensuring all stabilizers commute.

4.4.3 Virtual Logical Gates. Performing virtual logic gates in RASCqL’s ISA only requires a permutation of the physical data qubits that can usually be implemented as a virtual relabeling.

One concern is that such qubit relabelings may disturb existing structures our optimized syndrome extraction schedule exploits, and cause future QEC cycles to be slower. We show that this is not the case for the HGPS codes. First, the Dirty Cyclic Shifts operation requires a cyclic shift of the data qubits. Since HGPS is also cyclic, it is easy to see that this shift only modifies the ordering of future syndrome extraction cycles, but does not change the overall timing. The atom movement required for the autoCNOTs is a fold symmetry on the columns (rows). As we we show in Proposition

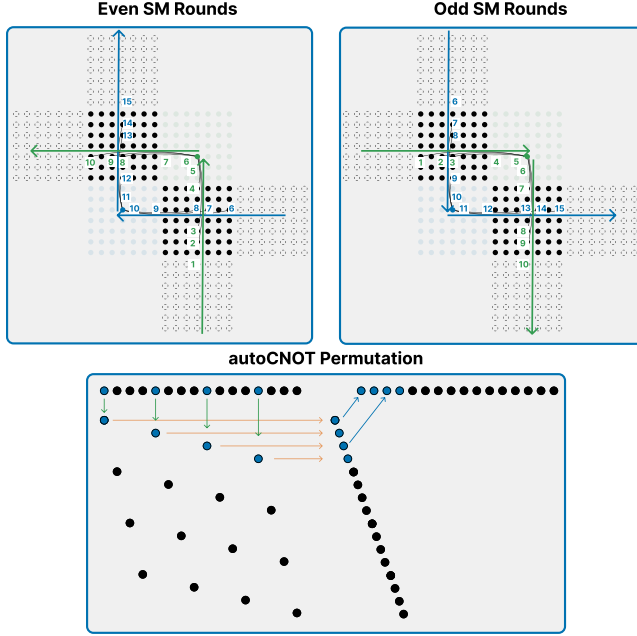


Figure 9. Top: Alternating movement schedule for syndrome measurement (SM) of the codes in RASCql. X/Z check qubit arrays (green/blue) are moved collectively along the defined path. Numbered stops for parallel 2Q gates indicate the position of an example X/Z check qubit. Bottom: Three AOD movements (green, orange, blue) that implements the qubit permutation for autoCNOTs, which only needs to be executed before tCNOTs.

C.2, this symmetry preserves the stabilizers exactly, hence requiring no changes to future syndrome extraction cycles.

We may need to implement the permutation physically when performing a tCNOT that involves a relabeled patch. We can also show that when combined with atom rearrangements for the tCNOT operations, permutations from virtual relabeling can be implemented efficiently. For the Dirty Cyclic Shifts, it suffices to move one column (row) before a tCNOT, leading to at most 1.2 ms delay. For autoCNOTs, three additional movements are needed to rearrange the grid. We can describe it for the first qubit in each column (row), which we label with two indices x, y such that qubit $i = 4x + y$, and suppose the initial position of qubit i are $(i, 0)$. The three movements are $(4a + b, 0) \mapsto (4a + b, 4b + a) \mapsto ((4a + b)/16, 4b + a) \mapsto (4b + a, 0)$, where the last step can be combined with the tCNOT. See Figure 9 for a visual illustration.

4.5 Resource State Management

4.5.1 State-mediated Reactive Operations. For adders and quantum look-up tables, Toffoli gates are implemented using $|T\rangle$ state injections, which may require S corrections. The reason we use $|T\rangle$ instead of $|CCZ\rangle$ states is that it's

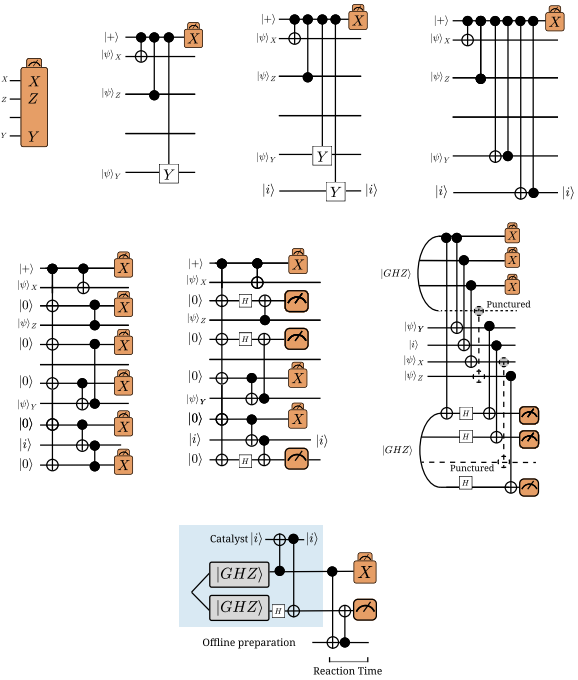


Figure 10. Preparation and consumption of a catalyzed GHZ state for reactive measurements. When a catalyzed GHZ state is available, it takes 2 tCNOTs (6 ms) to implement a reactive measurement. Online preparation, on the other hand, requires an additional 38.2 ms for $|GHZ\rangle$ preparation and 6 ms to use the catalyst.

easier to implement S corrections using $|i\rangle$ state catalysts than non-native CZ operations. These corrections may also depend on X errors from using Bell-pairs for parallelization. Rather than enforcing the correct measurement dependencies and implementing S -corrections on-the-fly, we can commute potential Clifford corrections to the end of the circuit, resulting in a weight-4 Pauli product measurement as shown in the final step of Figure 8. These reactive measurements can be implemented with two transversal CNOTs by consuming a special $|GHZ\rangle$ state (possibly prepared offline), as shown in Figure 10.

4.5.2 Reducing Provisioning Size. For the $[[450, 32, 8]]$ code, 8 MAJ blocks or temporary-AND Toffolis can be implemented in parallel. Each block may require reactive measurements parameterized by 5 measurement outcomes—two from the Bell-measurement of the previous MAJ block, and three from $|T\rangle$ injections—giving rise to $8 \times 2^5 = 256$ potential resource states to be requested. We reduce this number to a single type by allowing additional CQLU primitives.

Firstly, we arrange the logical qubit placement in CQLUs so the support of each reactive measurement is in the same

row or column. We prepare logical ancillae for only particular columns embedded in a block with $|0\rangle$ states, and use dirty cyclic shift to access the correct state. The layout may incur additional overhead for the logical computation, since bridge qubits used for parallelization participate in operations that belong to multiple blocks. Instead of assigning particular rows/columns to bridge qubits, we instead store them separately and SWAP them into the corresponding location before measurements, which can be done transversely and in parallel. We can again use dirty cyclic shifts for rearrangements when we embed the empty rows/columns with $|0\rangle$ eigenstates. Since any additional operation are done before measurements take place, it does not increase reaction time, and while it does increase the qubit footprint, the cost is not significant over the whole program due to the short lifespan of the additional qubits needed.

Secondly, we can split the measurement into X -and Z -terms and inject using two patches (where $Y = iXZ$), as illustrated in Figure 10. We can assume each qubit requires an X -term and a Z -term, and use virtual puncturing operations depending on the measurement results. This increases the reaction time by an additional transversal CNOT, but reduces the pool of potential states to 1. There is a caveat, however, when we use global transversal CNOTs for state-preparation: the Y terms require using a $|i\rangle$ catalyst, which requires a transversal CNOT and a transversal CZ onto the same qubit. While the CZ can be implemented as a CNOT conjugated by Hadamards, it also enacts a logical transpose on the encoded qubits, so we can only apply $CNOT_{i,j}$ and $CZ_{i,j}$ between qubit i, j in two blocks iff $i = j$. We overcome this by observing that each reactive measurement contains at most one Y -term; when we SWAP the bridge qubits into the i -th row/column, we can make sure that the Y term is in the i -th position, so the targets of both the CNOT and CZ is a qubit on the diagonal.

4.6 Scheduling and Pipelining State Generation

PReP allows us to decouple state generation from program execution with a small provision that contains catalyst $|i\rangle$ states on diagonal positions, and a pool of consumable $|T\rangle$ states and modified GHZ states. Another benefit of off-line preparation is now we can produce such states in batches with higher efficiency. For example, since GHZ states are prepared on only a single row/column, we can batch the preparations of 8 reactive-measurement ancillae together to save space-time cost. Another example is for magic states: rather than implanting two $[[15, 1, 3]]$ MSD in parallel in each block, we can use a $[[109, 19, 3]]$ over 4 blocks that require two additional global $tCNOT$ for a $2.6\times$ increase in per-logical state efficiency.

Finally, since request rate and amount is available prior to execution, we can in principle optimally schedule state generations per performance targets and device constraints.

To optimize fidelity or total active volume, we may generate states with an *as late as possible* policy, while the additional qubits required for state generation may drastically increase program footprint if request rates spike. On qubit-constrained devices, we may instead generate resource states at a constant rate to match program requirements on average; while able to maintain low-footprint, it may be required to halt program executions for resource states in certain request patterns. In this work, we adopt the latter strategy to retain the space advantage and assume the overhead, and leave more detailed optimization for future work.

5 Evaluation

5.1 Circuit level simulations

To estimate the performance and cost of RASCqL, we perform circuit-level simulations using Stim [71] and decode using BP-OSD. We use a standard circuit-level noise model where initialization and measurement experience bit-flip errors with probability p and one- and two-qubit gates cause depolarizing errors with probability p . To model the extra error introduced by movement-based automorphism gates and transversal operations, we insert an extra depolarizing error with probability p on the data qubits halfway through the experiment. Figure 11 shows the logical memory performance of HGPS codes for $r \in [3, 4, 5]$. We fit this data to the expect scaling behavior $p_L = A(bp)^{(d+1)/2}$, obtaining $A = 0.221 \pm 0.048$ and $b = 128.34 \pm 0.20$. Note an empirical threshold p_{th} is observed to be 0.78%. In comparison, we expect SHYPS (shown in Figure 12) to lack a clear threshold due to the increasing effect of measurement errors as code distance increases. We therefore fit the SHYPS data to the modified scaling function $p_L = A((b + cd)p)^{(d+1)/2}$, obtaining fit parameters $A = 0.1497$, $b = 0.3894$, and $c = 50.83$. We plot our fits for HGPS, SHYPS, Surface codes and compare them against those reported in [22] in Figure 13.

Finally, we simulate the injection of a quantum state from a $d = 3$ surface code into $r = 3$ and $r = 4$ HGPS codes using the universal adapter construction[72], decoding over 3 rounds of syndrome extraction, since we are limited by the surface code logical error rate. We simulate injecting the $|0\rangle$ and $|+\rangle$ states and combine the error rates to get the chance of either an X or Z error occurring on the injected state. The results are shown in Figure 14 and plotted against the HGPS memory experiment. We find that the combined error rate of the injection gadget is well-described by $p_{inj} = ap^2$ with $a = 3047 \pm 60$.

5.2 Resource estimation

5.2.1 GHZ State. Firstly, we compare the CQLU optimized $|GHZ\rangle$ preparation given in Figure 7 and with transversal surface code baseline in Figure 15. Benefiting from virtual operations and high rate, GHZ states can be prepared using CQLU instructions with more than $7\times$ reduction in qubit

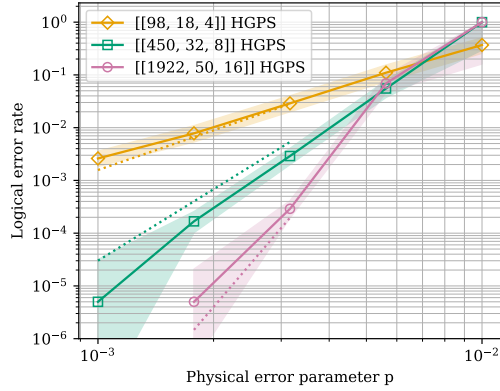


Figure 11. Logical Error Rate of HGPS under neutral atom inspire circuit level simulation. We account for additional idle and gate errors from transversal logical operations by inserting extra noise mechanisms in the middle of QEC cycles. We observe a threshold of around 0.78%.

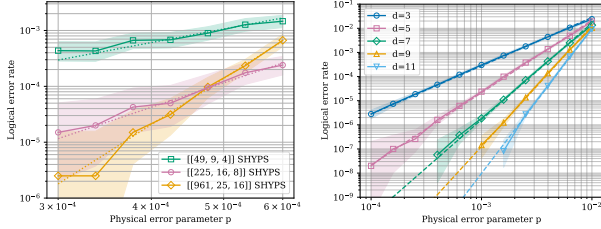


Figure 12. Logical Error Rate of SHYPS and Surface codes under neutral atom inspire circuit level simulation.

footprint, which translates to similar savings in terms of space time volume.

5.2.2 Magic State Distillation. We use a one- or two-level magic state distillation protocol using codes given in [11] and on HGPS with $r = 3, 4, 5, 6$ and concatenated HGPS with surface codes, and on surface codes with distances up to 45. We use a universal adapter to inject noisy magic states from small surface codes (see Figure 14) into the HGPS code. The per-state resource estimations are presented in Figure 16. Overall, we observe up to 2x footprint reduction, while the space-time volume can be 3x worse. We lose some footprint advantage due to the need for additional $|i\rangle$ states for X/Y reactive measurements, and the overall volume is worse, likely due to the low fidelity magic state injection protocol, requires us to use higher distance MSD protocols or multi-level protocols earlier than needed compared to surface code baselines.

While magic state cultivation [12] can be used for both RASCQL MSDs and the surface code baseline, RASCQL requires a universal adapter construction to make use of surface code cultivation, which adds substantial overhead and results in the lack of a clear benefit for RASCQL, as seen

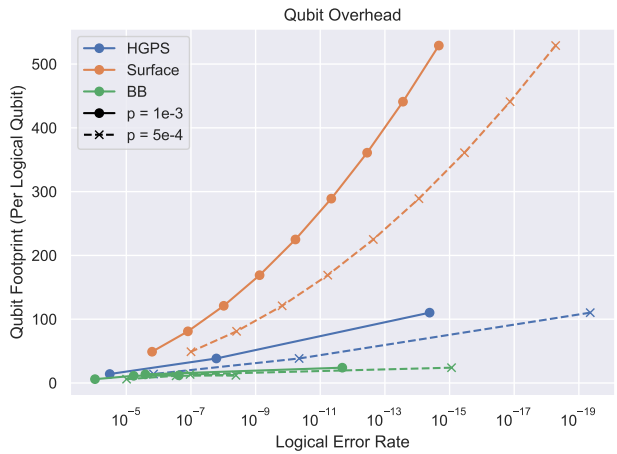
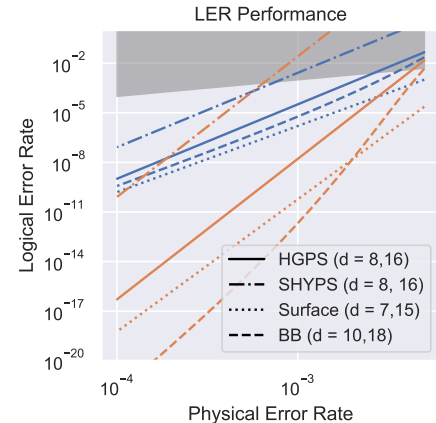


Figure 13. Top: Comparison between LER performance across HGPS (what our CQLU uses); SHYPS, a compute efficient subsystem code construction of the Simplex code [28]; the rotated surface code (our baseline)[7]; and Bivariate Bi-cycle code, hardware compatible qLDPC code with bi-planar checks[22]. Bottom: the projected per-logical qubit footprint for a range of target logical error rates.

in Figure 17. We expect the MSD volume may improve further by adapting similar post-selection techniques directly to qLDPC codes, but we leave this investigation for future work.

5.2.3 Adders. Finally, we compare implementations of adders on CQLUs against the surface code baseline in Figure 18. While each Q_4 can implement 8 MAJ blocks in parallel, the optimized surface code adder require 9 patches each (including 6 patches for CZ corrections that must be kept alive for sequential reactive measurements), leading to up to 7.84 \times difference in footprint, as reflected in the footprint comparison. For space-time volume, we evaluate the RASCQL adder with reaction-time $t_r = 3.9\text{ ms}$, the same as the logical cycle time, resulting in up to 1.25 \times reduction in

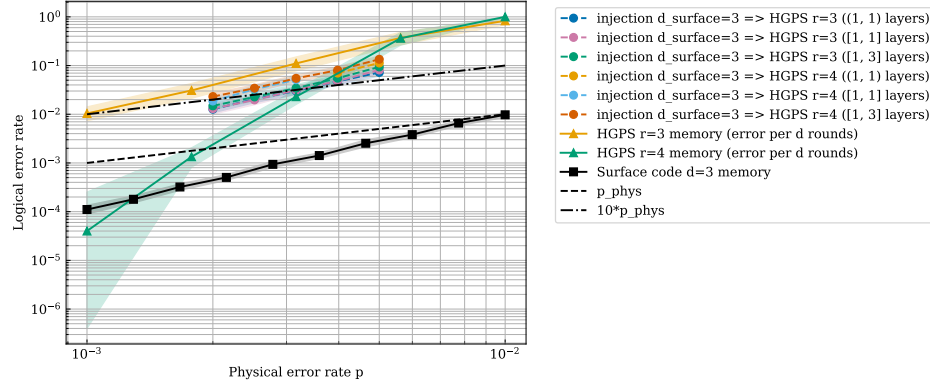


Figure 14. Logical error rate of injected magic states using universal adapters[72].

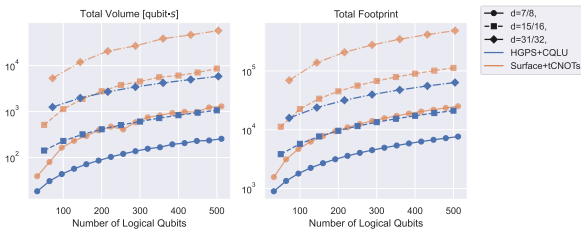


Figure 15. Space-time costs of producing a $|GHZ\rangle$.

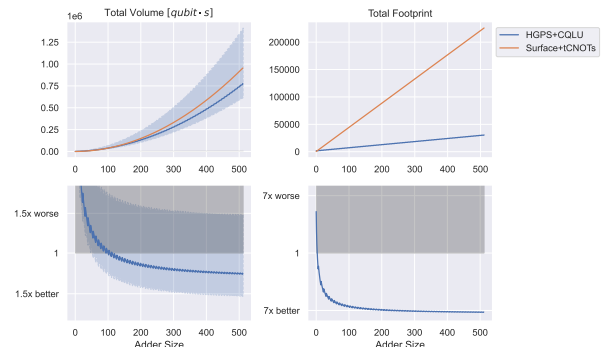


Figure 18. Space-time costs of adders using $HGPS_4$ and Surface code with $d = 7$. The shaded region represents the resource estimates with reaction time $t_r = 10\times$. Cost of magic states are not included in this analysis.

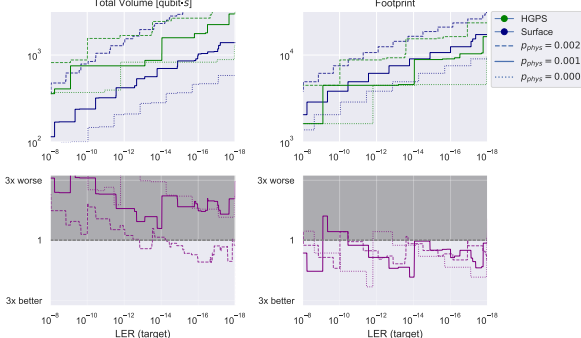


Figure 16. Space-time costs of producing high fidelity magic states in block.

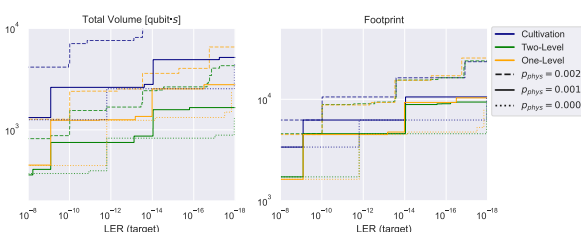


Figure 17. Comparison between concatenation schemes for MSD protocols.

Clifford volume. The Clifford volume is only 50% worse even with a reaction time 10 \times that of the surface code. Note that here we do not account for the cost to generate $|T\rangle$ states, since the scheduling and mapping of magic state production likely play a large role in the resulting resource estimation, which we leave for future work.

6 Discussions

In this paper, we proposed an architecture based on qLDPC codes with a logical ISA that implements specific functional subroutines such as state preparation and quantum arithmetic directly in block, with the potential to outperform surface code based architectures in qubit-footprint *and space-time volume*. In particular, we show an implementation of adders with reaction time limited operations that achieves up to a 7x reduction in footprint while also achieving space-time reduction in Clifford volume, and state factories with comparable costs to SoTA surface code baselines. This is achieved by carefully co-designing between circuit compilations at the functional layer, code and ISA constructions

at the logical layer, and RNAA realizations at the physical layer.

While our architecture has the capability to support subroutines used in practical algorithms, there remain several important gaps to scale our architecture to end-to-end resource estimation.

First, our reaction-time-limited model assumes efficient provisioning, storage, and routing of resource states, which may affect real end-to-end performance. A full-system scheduler that jointly optimizes footprint, latency, and state throughput is necessary to close this gap. Second, decoder latency plays a critical role. Although proposals for sub-millisecond qLDPC decoders exist [73], we conservatively assumed decoding time on the order of the QEC cycle (3.9 ms). A detailed sensitivity analysis across decoder latency, movement time, gate duration, and measurement overhead will be essential for realistic architectural comparisons.

Finally, while we focused on HGPS codes due to favorable RNAA embeddings and intrinsic symmetries, our code-modification framework applies broadly to other QECC families. A systematic search for compute-efficient qLDPC codes, co-optimizing automorphism structure, LDPC constraints, and hardware compatibility, may uncover architectures with improved flexibility across workloads and platforms.

Overall, RASCqL suggests a shift in perspective: rather than replicating a universal RISC-style ISA in qLDPC codes, or using them as quantum memory, we can instead treat them as specialized accelerators for dominant algorithmic subroutines. RASCqL establishes the question of how far this CISQ philosophy can scale toward full utility-level workloads.

7 Acknowledgments

We thank Yifan Hong for early discussions on Simplex codes that inspired the code modification constructions; Harry Zhou and Casey Duckering for helpful discussion on transversal architecture with reconfigurable neutral atom arrays; and Chris Kang for helpful discussions on reaction-time limited compilation. We also thank Chris Kang and Yifan Hong for their helpful feedback on the manuscript.

WY acknowledges support by the NSF GRFP Program under Grant No. 2023360346. FTC is the Chief Scientist for Quantum Software at Infleqtion. This work is funded in part by the STAQ project under award NSF Phy-232580; in part by the US Department of Energy Office of Advanced Scientific Computing Research, Accelerated Research for Quantum Computing Program; and in part by the NSF Quantum Leap Challenge Institute for Hybrid Quantum Architectures and Networks (NSF Award 2016136), in part by the NSF National Virtual Quantum Laboratory program, in part based upon work supported by the U.S. Department of Energy, Office of Science, National Quantum Information Science Research Centers, and in part by the Army Research Office under

Grant Number W911NF-23-1-0077. The views and conclusions contained in this document are those of the authors and should not be interpreted as representing the official policies, either expressed or implied, of the U.S. Government, or the National Science Foundation. The U.S. Government is authorized to reproduce and distribute reprints for Government purposes notwithstanding any copyright notation herein.

References

- [1] Peter W. Shor. Algorithms for quantum computation: Discrete logarithms and factoring. In *Proceedings of 35th Annual Symposium on Foundations of Computer Science (FOCS)*, pages 124–134, 1994.
- [2] Richard P. Feynman. Simulating physics with computers. *International Journal of Theoretical Physics*, 21:467–488, 1982.
- [3] Michael E. Beverland, Prakash Murali, Matthias Troyer, Krysta M. Svore, Torsten Hoefer, Vadym Kliuchnikov, Guang Hao Low, Matthias Soeken, Aarthi Sundaram, and Alexander Vaschillo. Assessing requirements to scale to practical quantum advantage. *arXiv preprint*, 2022.
- [4] Frank Arute, Kunal Arya, Ryan Babbush, Dave Bacon, Joseph C. Bardin, Rami Barends, and et al. Quantum supremacy using a programmable superconducting processor. *Nature*, 574:505–510, 2019.
- [5] Juan M. Pino, Joan M. Dreiling, Caroline Figgatt, John P. Gaebler, Steven A. Moses, and et al. Demonstration of the trapped-ion quantum ccd computer architecture. *Nature*, 592:209–213, 2021.
- [6] Dolev Bluvstein, Simon J. Evered, Alexandra A. Geim, Sophie H. Li, Hengyun Zhou, Tom Manovitz, Sepehr Ebadi, Madelyn Cain, Marcin Kalinowski, Dominik Hangleiter, J. Pablo Bonilla Ataides, Nishad Maskara, Iris Cong, Xun Gao, Pedro Sales Rodriguez, Thomas Karolyshyn, Giulia Semeghini, Michael J. Gullans, Markus Greiner, Vladan Vuletić, and Mikhail D. Lukin. Logical quantum processor based on reconfigurable atom arrays. *Nature*, 626(7997):58–65, 2024.
- [7] Austin G. Fowler, Matteo Mariantoni, John M. Martinis, and A. N. Cleland. Surface codes: Towards practical large-scale quantum computation. *Physical Review A*, 86(3):032324, 2012.
- [8] Dominic Horsman, Austin G. Fowler, Simon Devitt, and Rodney Van Meter. Surface code quantum computing by lattice surgery. *New Journal of Physics*, 14(12):123011, 2012.
- [9] Hengyun Zhou, Chen Zhao, Madelyn Cain, Dolev Bluvstein, Nishad Maskara, Casey Duckering, Hong-Ye Hu, Sheng-Tao Wang, Aleksander Kubica, and Mikhail D. Lukin. Low-overhead transversal fault tolerance for universal quantum computation, 2025.
- [10] Hengyun Zhou, Casey Duckering, Chen Zhao, Dolev Bluvstein, Madelyn Cain, Aleksander Kubica, Sheng-Tao Wang, and Mikhail D. Lukin. Resource analysis of low-overhead transversal architectures for reconfigurable atom arrays. In *Proceedings of the 52nd Annual International Symposium on Computer Architecture, SIGARCH ’25*, page 1432–1448. ACM, June 2025.
- [11] Jeongwan Haah and Matthew B. Hastings. Codes and protocols for distilling t, controlled-s, and toffoli gates. *Quantum*, 2:71, June 2018.
- [12] Craig Gidney, Noah Shutty, and Cody Jones. Magic state cultivation: growing t states as cheap as cnot gates, 2024.
- [13] Martin Ekera Craig Gidney. How to factor 2048 bit rsa integers in 8 hours using 20 million noisy qubits. *Quantum*, 5(433), 2021.
- [14] Daniel Litinski. How to compute a 256-bit elliptic curve private key with only 50 million toffoli gates, 2023.
- [15] Ryan Babbush, Craig Gidney, Dominic W. Berry, Nathan Wiebe, Jarrod McClean, Alexandru Paler, Austin Fowler, and Hartmut Neven. Encoding electronic spectra in quantum circuits with linear t complexity. *Phys. Rev. X*, 8:041015, Oct 2018.

[16] Daniel Litinski and Naomi Nickerson. Active volume: An architecture for efficient fault-tolerant quantum computers with limited non-local connections, 2022.

[17] Michael E. Beverland, Vadym Kliuchnikov, and Eddie Schoute. Surface code compilation via edge-disjoint paths. *PRX Quantum*, 3:020342, 2022.

[18] Daniel Litinski. A game of surface codes: Large-scale quantum computing with lattice surgery. *Quantum*, 3:128, 2019.

[19] Arpit Dua, Aleksander Kubica, Liang Jiang, Steven T. Flammia, and Michael J. Gullans. Clifford-deformed surface codes. *PRX Quantum*, 5:010347, Mar 2024.

[20] Shouzhen Gu, Alex Retzker, and Aleksander Kubica. Fault-tolerant quantum architectures based on erasure qubits. *Phys. Rev. Res.*, 7:013249, Mar 2025.

[21] Craig Gidney. How to factor 2048 bit rsa integers with less than a million noisy qubits, 2025.

[22] Sergey Bravyi, Andrew W. Cross, Jay M. Gambetta, Dmitri Maslov, Patrick Rall, and Theodore J. Yoder. High-threshold and low-overhead fault-tolerant quantum memory. *Nature*, 627(8005):778–782, March 2024.

[23] Qian Xu, J. Pablo Bonilla Ataides, Christopher A. Pattison, Nithin Ravveendran, Dolev Bluvstein, Jonathan Wurtz, Bane Vasić, Mikhail D. Lukin, Liang Jiang, and Hengyun Zhou. Constant-overhead fault-tolerant quantum computation with reconfigurable atom arrays. *Nature Physics*, 20:1084–1090, 2024.

[24] Joshua Viszlai, Willers Yang, Sophia Fuhui Lin, Junyu Liu, Natalia Nottingham, Jonathan M. Baker, and Frederic T. Chong. Matching generalized-bicycle codes to neutral atoms for low-overhead fault-tolerance, 2024.

[25] Samuel Stein, Shifan Xu, Andrew W. Cross, Theodore J. Yoder, Ali Javadi-Abhari, Chenxu Liu, Kun Liu, Zeyuan Zhou, Charles Quinn, Yufei Ding, Yongshan Ding, and Ang Li. Architectures for heterogeneous quantum error correction codes, 2024.

[26] Jérôme Guyot and Samuel Jaques. On the addressability problem on css codes, 2025.

[27] Hasan Sayginel, Stergios Koutsoumpas, Mark Webster, Abhishek Rajput, and Dan E. Browne. Fault-tolerant logical clifford gates from code automorphisms. *PRX Quantum*, 6:030343, Sep 2025.

[28] Alexander J. Malcolm, Andrew N. Glaudell, Patricio Fuentes, Daryus Chandra, Alexis Schotte, Colby DeLisle, Rafael Haenel, Amir Ebrahimi, Joschka Roffe, Armanda O. Quintavalle, Stefanie J. Beale, Nicholas R. Lee-Hone, and Stephanie Simmons. Computing efficiently in qldpc codes. *arXiv preprint*, 2025.

[29] Guang Hao Low and Isaac L. Chuang. Hamiltonian simulation by qubitization. *Quantum*, 3:163, July 2019.

[30] Matthew P. Harrigan, Tanuj Khattar, Charles Yuan, Anurudh Peduri, Noureldin Yosri, Fionn D. Malone, Ryan Babbush, and Nicholas C. Rubin. Expressing and analyzing quantum algorithms with qualtran, 2024.

[31] Vera von Burg, Guang Hao Low, Thomas Häner, Damian S. Steiger, Markus Reiher, Martin Roetteler, and Matthias Troyer. Quantum computing enhanced computational catalysis. *Physical Review Research*, 3(3), July 2021.

[32] Joonho Lee, Dominic W. Berry, Craig Gidney, William J. Huggins, Jarrod R. McClean, Nathan Wiebe, and Ryan Babbush. Even more efficient quantum computations of chemistry through tensor hypercontraction. *PRX Quantum*, 2(3), July 2021.

[33] András Gilyén, Yuan Su, Guang Hao Low, and Nathan Wiebe. Quantum singular value transformation and beyond: exponential improvements for quantum matrix arithmetics. In *Proceedings of the 51st Annual ACM SIGACT Symposium on Theory of Computing*, STOC ’19, page 193–204. ACM, June 2019.

[34] Athena Caesura, Cristian L. Cortes, William Pol, Sukin Sim, Mark Steudtner, Gian-Luca R. Anselmetti, Matthias Degroote, Nikolaj Moll, Raffaele Santagati, Michael Streif, and Christofer S. Tautermann. Faster quantum chemistry simulations on a quantum computer with improved tensor factorization and active volume compilation, 2025.

[35] Bryan Eastin and Emanuel Knill. Restrictions on transversal encoded quantum gate sets. *Physical Review Letters*, 102(11):110502, 2009.

[36] Sergey Bravyi and Alexei Kitaev. Universal quantum computation with ideal clifford gates and noisy ancillas. *Physical Review A*, 71(2), February 2005.

[37] Héctor Bombín and Miguel A Martin-Delgado. Optimal resources for topological two-dimensional stabilizer codes: Comparative study. *Physical Review A—Atomic, Molecular, and Optical Physics*, 76(1):012305, 2007.

[38] Anthony Leverrier, Jean-Pierre Tillich, and Gilles Zemor. Quantum expander codes. In *2015 IEEE 56th Annual Symposium on Foundations of Computer Science*, page 810–824. IEEE, October 2015.

[39] Theodore J. Yoder, Eddie Schoute, Patrick Rall, Emily Pritchett, Jay M. Gambetta, Andrew W. Cross, Malcolm Carroll, and Michael E. Beverland. Tour de gross: A modular quantum computer based on bivariate bicycle codes, 2025.

[40] Noah Berthelsen, Michael J. Gullans, Yifan Hong, Maryam Mudassar, and Shi Jie Samuel Tan. Automorphism gadgets in homological product codes, 2025.

[41] Qian Xu, Hengyun Zhou, Guo Zheng, Dolev Bluvstein, J. Pablo Bonilla Ataides, Mikhail D. Lukin, and Liang Jiang. Fast and parallelizable logical computation with homological product codes. *Phys. Rev. X*, 15:021065, May 2025.

[42] Vadym Kliuchnikov, Dmitri Maslov, and Michele Mosca. Practical approximation of single-qubit unitaries by single-qubit clifford and t circuits. *IEEE Transactions on Computers*, 65(1):161–172, 2016.

[43] Austin G. Fowler. Surface code resource estimation for magic state distillation. *arXiv preprint*, 2012.

[44] J. Eli Bourassa, Rafael N. Alexander, Michael Vasmer, Ashlesha Patil, Ilan Tzitrin, Takaya Matsuura, Daiqin Su, Ben Q. Baragiola, Saikat Guha, Guillaume Dauphinain, Krishna K. Sabapathy, Nicolas C. Menicucci, and Ish Dhand. Blueprint for a scalable photonic fault-tolerant quantum computer. *Quantum*, 5:392, February 2021.

[45] Jwo-Sy Chen, Erik Nielsen, Matthew Ebert, Volkan Inlek, Kenneth Wright, Vandiver Chaplin, Andrii Maksymov, Eduardo Páez, Amrit Poudel, Peter Maunz, and John Gamble. Benchmarking a trapped-ion quantum computer with 30 qubits. *Quantum*, 8:1516, November 2024.

[46] IBM Quantum Roadmap – Starling and Modular Processors. <https://www.ibm.com/roadmaps/quantum/andrelated2025IBMBlogannouncements>. IBM, accessed 2025-08-20.

[47] Hannah J. Manetsch, Gyohei Nomura, Elie Bataille, Xudong Lv, Kon H. Leung, and Manuel Endres. A tweezer array with 6,100 highly coherent atomic qubits. *Nature*, 647(8088):60–67, September 2025.

[48] Matt. J. Bedalov, Matt Blakely, Peter. D. Buttler, Caitlin Carnahan, Frederic T. Chong, Woo Chang Chung, Dan C. Cole, Palash Goiporia, Pranav Gokhale, Bettina Heim, Garrett T. Hickman, Eric B. Jones, Ryan A. Jones, Pradnya Khalate, Jin-Sung Kim, Kevin W. Kuper, Martin T. Lichtman, Stephanie Lee, David Mason, Nathan A. Neff-Mallon, Thomas W. Noel, Victory Omole, Alexander G. Radnaev, Rich Rines, Mark Saffman, Efrat Shabtai, Mariesa H. Teo, Bharath Thotakura, Teague Tomesh, and Angela K. Tucker. Fault-tolerant operation and materials science with neutral atom logical qubits, 2024.

[49] Rich Rines, Benjamin Hall, Mariesa H. Teo, Joshua Viszlai, Daniel C. Cole, David Mason, Cameron Barker, Matt J. Bedalov, Matt Blakely, Tobias Bothwell, Caitlin Carnahan, Frederic T. Chong, Samuel Y. Eubanks, Brian Fields, Matthew Gillette, Palash Goiporia, Pranav Gokhale, Garrett T. Hickman, Marin Iliev, Eric B. Jones, Ryan A. Jones, Kevin W. Kuper, Stephanie Lee, Martin T. Lichtman, Kevin Loeffler, Nate Mackintosh, Farhad Majdeteimouri, Peter T. Mitchell, Thomas W. Noel, Ely Novakoski, Victory Omole, David Owusu-Antwi, Alexander G.

Radnaev, Anthony Reiter, Mark Saffman, Bharath Thotakura, Teague Tomesh, and Ilya Vinogradov. Demonstration of a logical architecture uniting motion and in-place entanglement: Shor's algorithm, constant-depth cnot ladder, and many-hypercube code, 2025.

[50] Lov K. Grover. A fast quantum mechanical algorithm for database search. In *Proceedings of the 28th Annual ACM Symposium on Theory of Computing (STOC)*, pages 212–219, 1996.

[51] Edward Farhi, Jeffrey Goldstone, and Sam Gutmann. A quantum approximate optimization algorithm. *arXiv preprint*, 2014.

[52] Yuval R. Sanders, Dominic W. Berry, Pedro C.S. Costa, Louis W. Tessler, Nathan Wiebe, Craig Gidney, Hartmut Neven, and Ryan Babbush. Compilation of fault-tolerant quantum heuristics for combinatorial optimization. *PRX Quantum*, 1:020312, Nov 2020.

[53] Bela Bauer, Sergey Bravyi, Mario Motta, and Garnet Kin-Lic Chan. Quantum Algorithms for Quantum Chemistry and Quantum Materials Science. *Chemical Reviews*, 120(22):12685–12717, November 2020.

[54] Ashley Montanaro. Quantum algorithms: an overview. *npj Quantum Information*, 2(1):15023, January 2016.

[55] M. Cerezo, Andrew Arrasmith, Ryan Babbush, Simon C. Benjamin, Suguru Endo, Keisuke Fujii, Jarrod R. McClean, Kosuke Mitarai, Xiao Yuan, Lukasz Cincio, and Patrick J. Coles. Variational quantum algorithms. *Nature Reviews Physics*, 3(9):625–644, August 2021.

[56] Aram W. Harrow, Avinatan Hassidim, and Seth Lloyd. Quantum algorithm for linear systems of equations. *Phys. Rev. Lett.*, 103:150502, Oct 2009.

[57] Craig Gidney. Windowed quantum arithmetic, 2019.

[58] Joonho Lee, Dominic W. Berry, Craig Gidney, William J. Huggins, Jarrod R. McClean, Nathan Wiebe, and Ryan Babbush. Even more efficient quantum computations of chemistry through tensor hypercontraction. *PRX Quantum*, 2:030305, Jul 2021.

[59] Guang Hao Low and Isaac L. Chuang. Hamiltonian Simulation by Qubitization. *Quantum*, 3:163, July 2019.

[60] Craig Gidney. Halving the cost of quantum addition. *Quantum*, 2:74, June 2018. arXiv:1709.06648 [quant-ph].

[61] Guang Hao Low, Vadym Kliuchnikov, and Luke Schaeffer. Trading T gates for dirty qubits in state preparation and unitary synthesis. *Quantum*, 8:1375, June 2024.

[62] A. M. Steane. Error correcting codes in quantum theory. *Phys. Rev. Lett.*, 77:793–797, Jul 1996.

[63] Nikolas P. Breuckmann and Simon Burton. Transversal automorphism-based logical gates in qldpc codes. *arXiv preprint*, 2024.

[64] Austin G. Fowler. Time-optimal quantum computation, 2013.

[65] Alexander Cowtan, Zhiyang He, Dominic J. Williamson, and Theodore J. Yoder. Parallel logical measurements via quantum code surgery, 2025.

[66] Jean-Pierre Tillich and Gilles Zémor. Quantum ldpc codes with positive rate and minimum distance proportional to \sqrt{n} . *IEEE Transactions on Information Theory*, 60(2):1193–1202, 2014.

[67] Willers Yang and Patrick Rall. Harnessing the power of long-range entanglement for clifford circuit synthesis. *IEEE Transactions on Quantum Engineering*, 5:1–10, 2024.

[68] Craig Gidney. Halving the cost of quantum addition. *Quantum*, 2:74, June 2018.

[69] Shraddha Anand, Conor E Bradley, Ryan White, Vikram Ramesh, Kevin Singh, and Hannes Bernien. A dual-species rydberg array. *Nature Physics*, 20(11):1744–1750, 2024.

[70] Argyris Giannisis Manes and Jahan Claes. Distance-preserving stabilizer measurements in hypergraph product codes. *Quantum*, 9:1618, 2025.

[71] Craig Gidney. Stim: a fast stabilizer circuit simulator. *Quantum*, 5:497, July 2021.

[72] Esha Swaroop, Tomas Jochym-O'Connor, and Theodore J. Yoder. Universal adapters for quantum ldpc codes. *arXiv preprint*, 2025.

[73] Tristan Müller, Thomas Alexander, Michael E. Beverland, Markus Bühler, Blake R. Johnson, Thilo Maurer, and Drew Vandeth. Improved belief propagation is sufficient for real-time decoding of quantum memory, 2025.

[74] Armanda O. Quintavalle, Paul Webster, and Michael Vasmer. Partitioning qubits in hypergraph product codes to implement logical gates. *Quantum*, 7:1153, October 2023.

A Preliminary

In this section, we write down the notations used for quantum codes and logical operations, as well as definition for the Simplex code and its quantum product variants. We also survey some useful facts and propositions from prior work as they may aid understanding of main results.

A.1 General Notations

Definition 1 (Binary vector space). *Let \mathbb{F}_2^n denote an n dimensional binary vector space. Binary matrices $M \in \mathbb{F}_2^{r \times c}$, with r rows and c columns, are used to represent linear operators or a subspace defined by its rows. Furthermore, let $\text{Rows}(M) = \{w_1, \dots, w_r\}$ and $\text{Cols}(M) = \{v_1, \dots, v_n\}$ refer to row- and column- vectors of M , we use $\langle M \rangle = \langle \text{Rows}(M) \rangle$, and $\langle M \rangle^\perp = \{x : Mx = 0\} \subset \mathbb{F}_2^n$ to denote the rowspace and nullspace of M , which we may refer to as M, M^\perp with a slight abuse of notations.*

Definition 2 (Hilbert space). *The state vector of a qubit can be described by a unit vector on the complex plane \mathbb{C}^2 . The state space of n qubits is described by the 2^n dimensional Hilbert space $\mathbb{H}^n = (\mathbb{C}^2)^{\otimes n}$. We refer to \mathbb{H}^n as a n -qubit Hilbert space, and a 2^k dimensional subspace as a k -qubit subspace.*

We can construct new matrices by stacking $M' = \begin{bmatrix} M_1 & M_2 \\ M_3 & M_4 \end{bmatrix}$.

Following conventions in literature, a delineator may be added when stacking two matrices $M' = [M_1 | M_2]$. We use \otimes to denote Kronecker product, and \oplus to denote direct sum (as opposed to the Kronecker sum): $M_1 \oplus M_2 = \begin{bmatrix} M_1 & \\ & M_2 \end{bmatrix}$. Finally, we say M is w -bounded if $\text{wt}(c) \leq w \forall c \in \text{Rows}(M)$.

Definition 3 (Binary Linear Code). *A $[n, k, d]$ binary linear code C is a k -dimensional subspace of \mathbb{F}_2^n s.t. $\min_{c \in C} \text{wt}(c) \geq d$. C is specified by:*

1. a generator matrix $G \in \mathbb{F}_2^{n_k \times n}$ where $C = \langle G \rangle$, the row-space of G . Rows of G can be interpreted as a basis for the codewords in C .
2. a check matrix $H \in \mathbb{F}_2^{n_c \times n}$ where $C = \langle H \rangle^\perp$. Rows of H can be interpreted as parity checks on the codewords.

We use $C(G, H)$ to denote a classical code with generator matrix G and check matrix H .

As constraining to each independent parity check being 0 removes a degree of freedom from the vector space, we have $\dim(G) = n - \dim(H)$, $\dim(H) = n - k$. Since $\text{Rows}(G)$ spans the null space of H , also have that $HG^T = 0$, and $\langle G \rangle \cap \langle H \rangle = e_0$. Finally, we note that there may exist many choices of G and H with $n_k \geq k$ and $n_c \geq n - k$. Choices of H, G satisfying specific criterion will become a motif in following studies.

Definition 4 (CSS Code). *A $[[n, k, d]]$ quantum CSS code Q is a k -qubit subspace of \mathbb{H}^n such that any two distinct codewords differ by a Pauli operator of weight at least d . Q contains*

states stabilized by a set of Pauli operators $S = S_X \sqcup S_Z$; that is, $Q = \{|\psi\rangle |P|\psi\rangle = |\psi\rangle \forall P \in S\}$. More compactly, Q can be specified by:

1. two classical binary linear codes $C_X, C_Z \subset \mathbb{F}_2^n$ with $C_Z^\perp \in C_X$, where C_X, C_Z defines the X, Z observables of Q .
2. two check matrices $H_X \in \mathbb{F}_2^{n_X \times n}, H_Z \in \mathbb{F}_2^{n_Z \times n}$ with $H_X H_Z^T = 0$, where H_X, H_Z defines the S_X, S_Z stabilizers.

A.2 Hypergraph Product Codes

A simple way to construct quantum codes is by taking tensor-products of two classical codes with the identity. We obtain a quantum CSS code as a result which we call a hypergraph product code, or HGP for short:

Definition 5 (Hypergraph Product (HGP) Code). *Given two classical codes $\{C_i\}_{i=0,1}$ with H_i , parameters $[n_i, k_i, d_i]$, and generators G_i as seeds, and let C'_i be the code obtained with checks H_i^T , parameters $[m_i, k'_i, d'_i]$, and generators G'_i , we can construct a quantum hypergraph product code Q_{HGP} with stabilizer checks:*

$$H_X = [H_1 \otimes I_{n_2} | I_{m_1} \otimes H_2^T], \quad (10)$$

$$H_Z = [I_{n_1} \otimes H_2 | H_1^T \otimes I_{m_2}]. \quad (11)$$

Furthermore, Q_{HGP} has parameters

$$n = n_1 n_2 + m_1 m_2 \quad (12)$$

$$k = k_1 k_2 + k'_1 k'_2 \quad (13)$$

$$d = \min(d_1, d_2, d'_1, d'_2), \quad (14)$$

and canonical basis of logical operators [74]:

$$G_X = [P(H_1) \otimes G_2 | 0^{m_1 m_2 \times m_1 n_2}] \oplus [0^{n_1 m_2 \times n_1 n_2} | G'_1 \otimes P(H_2^T)] \quad (15)$$

$$G_Z = [G_1 \otimes P(H_2) | 0^{m_1 m_2 \times m_1 n_2}] \oplus [0^{n_1 m_2 \times n_1 n_2} | P(H_1^T) \otimes G'_2], \quad (16)$$

where G_i, G'_i is in the reduced-row-echelon form, and $P(H)$ is constructed using the pivots of G such that $PG^T = I$.

A.3 Logical Operations

In the broadest definition, a logical operation refers a transformation of the data (qu)bits that preserves the code. Here we are interested in logical operations that are both non-trivial and distance preserving. If we assume qubit permutations are noiseless (which is especially the case when a virtual relabeling of qubit position suffices), the resulting logical operations are trivially distance preserving. We call these operations code automorphisms:

Definition 6 (Automorphisms in Classical Codes). *Given a code $C(G, H)$, $\sigma \in \mathbb{P}_k$ is a code automorphism if $\exists g \in \mathbb{GL}_k(\mathbb{F}_2)$ s.t.*

$$G\sigma = gG. \quad (18)$$

g , referred to as the automorphism gate, describe the logical action of the code automorphism under the basis defined by G .

There are some useful facts we can show about code automorphisms. These facts follow from several propositions in [40] but are also to establish intuition. We survey some of these facts here in our notations.

Fact 1 (Automorphism group). *Given a code $C(G, H)$ and automorphisms Σ that preserves C (i.e. right action by $\sigma \in \Sigma$ is an isomorphism from C onto itself); Σ is a group under multiplication. We say \mathcal{G}_Σ is the automorphism group of C , or $\text{Aut}(C) = \mathcal{G}_\Sigma$, if*

$$\mathcal{G}_\Sigma \cong \{\sigma : \exists g \in \text{GL}_k(\mathbb{F}_2) \text{ s.t. } G\sigma = gG\}. \quad (19)$$

Proof. Clearly the identity preserves C , composing two isomorphisms lead to another isomorphism C , and compositions are associative as matrix multiplication is associative. For any $g, \sigma : G\sigma = gG$, we have that

$$G\sigma = gG \implies g^{-1}gG\sigma = g^{-1}G\sigma^2 \implies G\sigma^T = g^{-1}G, \quad (20)$$

hence σ^T preserves C , with $\sigma\sigma^T = I$. \square

Fact 2 (Automorphism Gate). *Given a code $C(G, H)$. Let $\mathcal{L}_G(C) = \{g : \exists \sigma \text{ s.t. } gG = G\sigma\}$ be the set of automorphism gates. Then, $\mathcal{L}_G(C)$ is a group, $\mathcal{L}_G(C) \cong \text{Aut}(C)$ if columns of G is unique.*

Proof. It's simple to show that $\mathcal{L}_G(C)$ is a group.

We can show that the mapping $\phi_G : \text{Aut}(C) \rightarrow \mathcal{L}_G$ s.t. $\phi_G(\sigma) = g \iff gG = G\sigma$ is an group homomorphism. Indeed, $\sigma_1G = g_1G, \sigma_2G = g_2G \implies \sigma_1\sigma_2G = g_1g_2G \implies \phi_G(\sigma_1\sigma_2) = g_1g_2$.

When columns of G are unique, $\ker \phi_G = I$ since any non-trivial permutation lead to non-trivial logical actions; ϕ_G is in fact an isomorphism. \square

Unless otherwise specified, we will assume columns of G are unique, in which case the notation $\text{Aut}(\cdot)$ is used synonymously to refer to the automorphism group or the group of resulting logical actions. In cases where non-unique columns are important for distance guarantees, we can keep track of how many times a particular column is duplicated before removing them, perform the code modification, and then duplicate the same column after modification.

Fact 3 (Automorphism of Checks). *Given $C(G, H)$ and $\sigma \in \text{Aut}(C)$, we also have that*

$$\exists h \in \text{GL}_k(\mathbb{F}_2) \text{ s.t. } H\sigma = hH. \quad (21)$$

Furthermore, we say σ is a matrix automorphism if $h \in \mathbb{P}_k$.

This follows from the fact that $C = \ker H$, and $\sigma(c) \in C \forall c \in C \implies H(\sigma(c))^T = (H\sigma^T)c^T = 0 \forall c \in C \implies \langle H \rangle = \langle H\sigma^T \rangle$.

r	3	4	5	6
H_r	$I + x + x^3$	$I + x + x^4$	$I + x^2 + x^5$	$I + x + x^6$

Table 3. Check matrices for the simplex code, where x denote the cyclic permutation matrix of dimension $2^r - 1$.

A.4 Simplex Codes and Quantum Variants

A classical code with expansive automorphism group is the simplex code:

Definition 7 (Simplex Codes). *An r -dimensional binary simplex code \mathcal{S}_r is a $[2^r - 1, r, 2^{r-1}]$ classical linear code with generator matrix G_r s.t.*

$$\text{Cols}(G_r) = \{b_1, \dots, b_{2^r - 1}\} \quad (22)$$

where elements of b_i correspond to digits of i in binary. Unless otherwise specified, let the check matrix be given as cyclic matrices in 3.

Definition 8 (Hypergraph Product of Simplex (HGPS) Codes). *Let \mathcal{S}_r, H_r be defined as 7. Define $Q_{\text{HGPS}, r}$ as the hypergraph product code with seeds H, H^T :*

$$H_X = [H \otimes I | I \otimes H^T] \quad (23)$$

$$H_Z = [I \otimes H | H^T \otimes I]. \quad (24)$$

$Q_{\text{HGPS}, r}$ has parameters $[(2(2^r - 1)^2, 2r^2, 2^{r-1})]$ and generators

$$G_X = [P \otimes G] \oplus [G \otimes P], \quad (25)$$

$$G_Z = [G \otimes P] \oplus [P \otimes G]. \quad (26)$$

$$(27)$$

Note the logical operators naturally partitions into two sets with disjoint support on the left and right sector.

A.5 Automorphism group of the Simplex codes

It is well known that the automorphism group of the Simplex code contains all linear transformations. This in fact saturates the upper-bound on the possible automorphism group size in any codes with the same number of logical bits, as a result of Corr 3.3 in [40].

Fact 4 (Simplex Automorphism). *Let \mathcal{S}_r be defined as in Def 7. Then, $\mathcal{L}_G(\mathcal{S}_r) = \text{GL}_r(\mathbb{F}_2)$.*

While HGPS do inherit all logical gates corresponding to the product of Simplex automorphisms by construction, the physical transformations required remains physical permutations (an hence fault tolerant) only if the classical automorphism is also a matrix automorphism on the checks, which is not true in general [40].

One approach to get around this, as proposed in [40], is to gauge out all problematic logical qubits:

Proposition A.1 (Left Sector HGPS Automorphism). *From $Q_{\text{HGPS}, r}$ as defined as in 8, we can obtain a subsystem code*

$Q_{HGPS,r}^L$, the left-sector HGPS, where logical qubits supported on the right sector is designated as gauge qubits. We have:

$$\mathbb{GL}_r(\mathbb{F}_2) \times \mathbb{GL}_r(\mathbb{F}_2) \leq \mathcal{L}_G(Q_{HGPS,r}^L). \quad (28)$$

i.e., for all $g = g_1 \otimes g_2 \in \mathbb{GL}_r(\mathbb{F}_2) \times \mathbb{GL}_r(\mathbb{F}_2)$, $\exists \sigma = \sigma_1 \otimes \sigma_2, h = h_1 \otimes h_2$, such that the action of $\sigma \oplus h$ on the physical qubits applies the logical transformation

$$\begin{aligned} G_X^L \sigma &= g G_X^L \\ G_Z^L \sigma &= g^{-T} G_Z^L \end{aligned}$$

fault-tolerantly to the logical qubits supported on the left sector.

The proof follows from [Theorem 5.5, 66] and [Lemma VIII.12, 28], which we survey here.

Proof. Given g_1, g_2 , we can choose

$$\begin{aligned} \sigma_1 : g_1^{-T} G &= G \sigma_1, \\ \sigma_2 : g_2 G &= G \sigma_2, \\ h_1 : h_1 H &= H \sigma_1, \\ h_2 : h_2^{-T} H &= H \sigma_2. \end{aligned}$$

Indeed, we can check that the stabilizers are preserved:

$$\begin{aligned} H_X \sigma \oplus h &= [H \sigma_1 \otimes \sigma_2 | h_1 \otimes H^T h_2] \\ &= [H \sigma_1 \otimes \sigma_2 | h_1 \otimes (h_2^T H)^T] \\ &= [h_1 H \otimes \sigma_2 | h_1 \otimes \sigma_2 H^T] \\ &= h_1 \otimes \sigma_2 H_X \\ H_Z \sigma \oplus h^{-T} &= [\sigma_1 \otimes H \sigma_2 | H^T h_1^{-T} \otimes h_2^{-T}] \\ &= [\sigma_1 \otimes H \sigma_2 | (h_1^{-1} H)^T \otimes h_2^{-T}] \\ &= [\sigma_1 \otimes h_2^{-T} H | \sigma_1 H^T \otimes h_2^{-T}] \\ &= \sigma_1 \otimes h_2^{-T} H_Z. \end{aligned}$$

Then, to show that σ leads to the desired logical action on the left sector, we first note that

$$I = P \sigma_1 \sigma_1^T G^T = P \sigma_1 G^T g_1^{-1} \quad (29)$$

$$\implies P \sigma_1 G^T = g_1 = g_1 P G^T \quad (30)$$

$$\implies (P \sigma_1 - g_1 P) G^T = 0 \quad (31)$$

$$\implies P \sigma_1 = g_1 P + M \quad (32)$$

for some $M \in \ker(G) = \langle H \rangle \implies M = aH$ for some matrix a . Then, it follows that

$$G_X^L \sigma = P \sigma_1 \otimes G \sigma_2 \quad (33)$$

$$= g_1 P \otimes g_2 G + aH \otimes G \quad (34)$$

$$= g G_X^L + a'(H_X + H_X^R), \quad (35)$$

where $a' = a \otimes G$ and H_X^R correspond to a transformation on right sector qubit, which does not effect the left sector logical operators. We can similarly show that $G_Z^L \sigma \simeq g^{-T} G_Z^L$ up to stabilizers and right-sector operations.

Finally, these automorphism gates are fault-tolerant. While implementations of h require entangling gates and decrease

the distance in general, it only effects qubits supported on the right sector, which we preemptively designated as gauge qubits. With, all logical observables being disjoint from physical qubits where entangling gates are applied, the distance of the dressed operators cannot decrease. \square

With these operators, $Q_{HGPS,r}^L$ can implement arbitrary CNOT-type operators efficiently using the synthesis routine shown in [28] with doubled qubit overhead. This approach unfortunately cannot implement diagonal gates.

B Code Modifications

Now, we have a language to describe the gap. Firstly, while having rich classical automorphisms are helpful for quantum computation, it also implies a poor encoding rate. This is often unnecessary as much smaller subset of gates usually suffice for any *practical* computation, leading to a natural question of whether we can design codes with better or constant encoding rates that contain exactly the gates we need. We investigate this question in section B.1, and show precise bounds on the number of physical qubits that suffices to augment automorphisms to a given code. Secondly, access to classical automorphisms isn't helpful unless we can lift them to quantum codes, and existing approaches either sacrifices LDPC property for a specific class of code or throw away up to half of the logical qubits. It is hence another important question to study resource efficient methods to lift specific classical automorphisms. We explore this question in section B.2. Specifically, we find minimal modifications of the checks such that automorphism are converted to matrix automorphisms that can be implemented virtually.

B.1 Prescribing Automorphisms

The equivalent definition for the group of automorphism gates using group action is as follows:

Proposition B.1 (Automorphism Condition). *Let us be given a classical linear code $C(G, H)$ and $\mathcal{G} = \{g_1, \dots, g_m\} \leq \mathbb{GL}_k(\mathbb{F}_2)$. Then, $\mathcal{G} \leq \mathcal{L}_G(C)$ iff*

$$\text{Orb}_{\mathcal{G}}^L(c) = \{g \cdot c \mid g \in \mathcal{G}\} \subseteq \text{Cols}(G) \quad \forall c \in \text{Cols}(G). \quad (36)$$

i.e. the columns of G is \mathcal{G} -invariant under left action.

This is simply a re-statement Definition 6, since $\text{Cols}(gG) = \text{Cols}(G\sigma) = \text{Cols}(G) \iff g \in \mathcal{L}_G(C)$. This definition gives a general way to construct codes with a prescribed automorphism group:

Theorem 3 (Automorphism Completion). *Let us be given a $[n, k, d]$ code $C(G, H)$ and $\mathcal{G} = \{g_1, \dots, g_m\} \leq \mathbb{GL}_k(\mathbb{F}_2)$. There exists a family of $[n' \leq nm, k, d' \leq dm]$ codes $C_{\mathcal{G}}(G_{\mathcal{G}}, H_{\mathcal{G}})$ such that $C \cong C_{\mathcal{G}}$, $\mathcal{G} \leq \mathcal{L}_{G_{\mathcal{G}}}(C_{\mathcal{G}})$.*

Proof. Simply take $G_{\mathcal{G}} = [g_1 G \cdots | g_m G]$ to achieve $n' = nm, d' = dm$. Then, non-unique columns can be punctured while preserving the automorphism group, simultaneously reducing both code length and distance.

To upper-bound the redundancy, we can find the smallest G -invariant set containing $\text{Cols}(G)$: $O = \mathcal{G} \cdot \text{Cols}(G) = \bigcup_{c \in \text{Cols}(G)} \text{Orb}_{\mathcal{G}}^L(c)$. It suffices to take G_O constructed by stacking all columns $c \in O$.

To find $H_{\mathcal{G}}$, we can assume WLOG that $G = [I|M]$, and let $M_O = G_O \setminus \text{Cols}(I_k)$; this gives

$$G_{\mathcal{G}} = [I \quad M_O] \quad (37)$$

$$H_{\mathcal{G}} = [M_O^T \quad I], \quad (38)$$

s.t. $H_{\mathcal{G}}G_{\mathcal{G}}^T = 2M_O^T = 0$. Hence, $C_{\mathcal{G}}(G_{\mathcal{G}}, H_{\mathcal{G}})$ defines a valid linear code.

It's also easy to check that $\text{Cols}(G_{\mathcal{G}}) = O$ is \mathcal{G} -invariant under left action: for all $c \in O$, $c = g_G \cdot c_G$ for some $g_G \in \mathcal{G}$, $c_G \in \text{Cols}(G)$, it follows $g \cdot c = g \cdot g_G \cdot c_G \in \text{Orb}_{\mathcal{G}}^L(c) \in O$ for all $g \in \mathcal{G}$. This implies $\mathcal{G} \leq \mathcal{L}_{G_{\mathcal{G}}}(C_{\mathcal{G}})$ by Prop B.1 \square

Note depending on \mathcal{G} , the size of the code grows with the size of the automorphism group we want to expand to. On one extreme, expanding the automorphism to $\text{GL}_k(\mathbb{F}_2)$ potentially yield an exponential increase in code length; in fact, starting with any code C , the $C_{\text{GL}_k(\mathbb{F}_2)}$ we obtain (after removing redundancy) is exactly the simplex code \mathcal{S}_r , with $n = 2^k - 1$. On the other hand, if we fix \mathcal{G} to be small, e.g. $\mathcal{G} = \{I, g_{\text{CNOT}}\}$ correspond to a single CNOT, we can obtain sharper guarantees on n', d' .

The code expansion given in Theorem 3 can maintain LDPC properties of the original check matrix if either the prescribed automorphism group is small, or if the group elements are sparse:

Theorem 4 (LDPC). *Let us be given a code $C(G, H)$ and $\mathcal{G} \leq \text{GL}_k(\mathbb{F}_2)$. Suppose H is w -bounded, g is t -bounded for all $g \in \mathcal{G}$ and $|\mathcal{G}| = m$. Then, the family of codes $C_{\mathcal{G}}(G_{\mathcal{G}}, H_{\mathcal{G}})$ given by Theorem 3 has a $(w + t + 1)$ -bounded check matrix $H_{\mathcal{G}}^{(t)}$ and a $(w + m + 1)$ -bounded check matrix $H_{\mathcal{G}}^{(m)}$.*

Proof. Let us find P_G, σ_G by Gaussian Elimination such that $G' = P_G G \sigma_G = [I|M]$ is in the canonical basis. Note both $H' = [M^T|I]$ and $H \sigma_G$ are valid check matrices for G' , hence there exists a basis change such that $P_H [M^T|I] \sigma_G^T = H$. Let $H_1 = P_H M^T$, and $H_2 = P_H$, it follows that $H_1, H_2, [H_1|H_2] = H$ are all w -bounded.

Following Theorem 3, we can find the orbit of M under \mathcal{G} , $M_O = [g_1 \cdots g_m \quad M \quad g_1 M \cdots g_m M]$ and define $G_{\mathcal{G}} = [I|M_O]$, giving us a code $C_{\mathcal{G}}$ with desired automorphism group. It remains to find a $H_{\mathcal{G}}$ with LDPC properties.

We begin with a valid check matrix $H_{\mathcal{G}}^{(1)} = [M_O^T|I]$. First, let σ_r be permutation that swaps row i with row $i + mk + (n - k)$ for $i \leq mk$, and $P_0 = \begin{bmatrix} I & \\ M^T & I \end{bmatrix}$ so that $P_0 \cdot \begin{bmatrix} g_i^T & I \\ M^T g_i^T & I \end{bmatrix} = \begin{bmatrix} g_i^T & I \\ M^T & I \end{bmatrix}$. Define $P'_0 = P_0 \oplus P_0 \oplus \dots \oplus P_0 \oplus I$ and $P_a =$

$\sigma_r^T P'_0 \sigma_r$, we can do the following transformation to obtain:

$$H_{\mathcal{G}}^{(2)} = P_a \cdot \left[\begin{array}{c|c} g_1^T & I \\ \vdots & \ddots \\ g_m^T & I \\ \hline M^T & I \\ \vdots & \ddots \\ M^T g_m^T & I \end{array} \right] \quad (39)$$

$$= \left[\begin{array}{c|c} g_1^T & I \\ \vdots & \ddots \\ g_m^T & I \\ \hline M^T & I \\ M^T & I \\ \vdots & \ddots \\ M^T & I \end{array} \right] \quad (40)$$

Then, we can apply the basis change $P_b = I_{mk} \oplus P_H \oplus \dots \oplus P_H$ on the bottom half of $H_{\mathcal{G}}^{(2)}$, and obtain

$$H_{\mathcal{G}}^{(3)} = P_b H_{\mathcal{G}}^{(2)} \quad (41)$$

$$= \left[\begin{array}{c|c} g_1^T & I \\ \vdots & \ddots \\ g_m^T & I \\ \hline H_1 & P_H \\ H_1 & P_H \\ \vdots & \ddots \\ H_1 & P_H \end{array} \right] \quad (42)$$

If $m \leq t$, we can construct a $(w + m + 1)$ -bounded check matrix by applying g_i^{-T} to rows $[ik, (i + 1)k - 1]$, obtaining

$$H_{\mathcal{G}}^{(m)} = \left[\begin{array}{c|c} I & g_1^{-T} \\ \vdots & \ddots \\ I & g_m^{-T} \\ \hline H_1 & P_H \\ H_1 & P_H \\ \vdots & \ddots \\ H_1 & P_H \end{array} \right] \quad (43)$$

Finally, we construct a $(w + t + 1)$ -bounded check matrix. Let $P_i = \begin{bmatrix} I & \\ g_{i+1}^T g_i^{-T} & I \end{bmatrix}$ for $i = 1, \dots, k$ so that $P_i \cdot \begin{bmatrix} g_i^T & I \\ g_{i+1}^T & I \end{bmatrix} = \begin{bmatrix} g_i^T & I \\ g_{i+1}^T g_i^{-T} & I \end{bmatrix}$, then apply P_i to rows $[ik, (i + 2)k - 1]$,

giving us:

$$H_{\mathcal{G}}^{(t)} = \left[\begin{array}{cccc} g_1^T & I & & \\ & g_2^T g_1^{-T} & I & \\ & & \ddots & \\ & & & I \\ \hline H_1 & & & P_H \\ & H_1 & & P_H \\ & & \ddots & \\ & & & P_H \end{array} \right] \quad (44)$$

Which is $(w + t + 1)$ -bounded, since $g_{i+1}g_i^{-1} \in \mathcal{G}$ is t -bounded. \square

We can often find tighter bounds for specific classes of operations. We list a few here for example.

Corollary B.2 (Expansion: CNOT Fan-out). *Let us be given a $[n, k, d]$ code $C(G, H)$ and let H be w -bounded. Let g_f denote a fan-out operations on up to $w + 1$ bits. There exists a $[2n, k, 2d]$ code $C'(G', H')$ s.t. $g_f \in \mathcal{L}_{G'}(C')$, where $H_{\mathcal{G}}$ is $(w + 2)$ -bounded.*

Corollary B.3 (Expansion: Local Commuting CNOTs). *Let us be given a $[n, k, d]$ code $C(G, H)$ with w -bounded H and a set of m commuting CNOT gates $\mathcal{G} = \{g_1, \dots, g_m\}$ on t bits. Then, there exists $[nm, k, md]$ code $C_{\mathcal{G}}(G', H')$ with $(w + t + 1)$ -bounded $H_{\mathcal{G}}$ s.t. any circuits involving only \mathcal{G} can be performed virtually.*

B.2 Converting Automorphisms

A code automorphism is also a matrix automorphism if we find $H\sigma = \rho H$ for some $\rho \in \mathbb{P}_k$. The matrix automorphism condition can be equivalently stated as follows:

Proposition B.4 (Matrix Automorphism Condition). *Let us be given a classical linear code $C(G, H)$ and $\Sigma = \{\sigma_1, \dots, \sigma_m\} \leq \text{Aut}(C)$. Then, elements of Σ are also matrix automorphisms iff*

$$\text{Orb}_{\Sigma}^R(r) = \{r \cdot \sigma \mid \sigma \in \Sigma\} \subseteq \text{Rows}(H) \quad \forall r \in \text{Rows}(H). \quad (45)$$

i.e. the rows of H is Σ -invariant under right action.

[40] shows that any classical linear code C admits an exponentially large check matrix where all automorphisms are also matrix automorphisms. Indeed, there exist codes such as the simplex code that saturate this bound. However, in general, the size of the check matrix can be bounded by the size of automorphisms we wish to convert to matrix automorphisms:

Theorem 5 (Matrix Automorphism Conversion). *Let us be given a code $C(G, H)$ and $\Sigma = \{\sigma_1, \dots, \sigma_m\} \leq \mathbb{P}_k$ and $\Sigma \leq \text{Aut}(C)$. There exists $H_{\Sigma} \in \mathbb{F}_2^{n_r \times n}$ with $n_r \leq (n - k) \times m$ s.t. Σ is a group of matrix automorphism on H_{Σ} . Furthermore, if H is w -bounded, H_{Σ} is wm -bounded.*

Proof. We can take $H_{\Sigma} = [(H\sigma_1)^T | \dots | (H\sigma_m)^T]^T$ to obtain a check matrix with $n_r = (n - k) \times m$, and remove non-unique rows.

We can bound the number of rows removed similar to the proof of Theorem 3. The smallest Σ -invariant set containing $\text{Rows}(H)$ is the right orbit union

$$\mathcal{O} = \bigcup_{r \in \text{Rows}(H)} \text{Orb}_{\Sigma}^R(r) = \{r \cdot \sigma \mid r \in \text{Rows}(H), \sigma \in \Sigma\}, \quad (46)$$

which gives $H_{\mathcal{O}}$ constructed from stacking rows in \mathcal{O} . For each $r \in \mathcal{O}$, we have $r = \text{Orb}_{\Sigma}^R(r')$ for some $r' \in \text{Rows}(H)$, hence for any $\sigma \in \Sigma$, $r \cdot \sigma \in \text{Orb}_{\Sigma}^R(r') \in \mathcal{O} = \text{Rows}(H_{\mathcal{O}})$, and it follows $H_{\mathcal{O}}\sigma = \rho H_{\mathcal{O}}$ for all $\sigma \in \Sigma$. \square

The number of checks can be improved if the automorphism group was obtained through code expansion, and LDPC properties can still be maintained if both the size and the sparsity of prescribed automorphism is bounded :

Theorem 6 (Expanded Matrix Automorphism Conversion). *Let us be given $C(G, H)$ and $\mathcal{G} \leq \text{GL}_k(\mathbb{F}_2)$. Suppose H is w -bounded, g is t -bounded for all $g \in \mathcal{G}$ and $|\mathcal{G}| = m$. Then, there exists a family of $[[nm, k, dm]]$ codes $C_{\mathcal{G}}(G_{\mathcal{G}}, H_{\mathcal{G}})$ with a $(w + mt)$ -bounded check matrix $H_{\mathcal{G}}$ using $(m - 1)mk$ additional checks such that $g \in \mathcal{G}$ is a matrix automorphism for all $g \in \mathcal{G}$.*

Proof. Let $G_{\mathcal{G}} = [I \ g_1 \dots g_m \ M \ g_1M \dots g_mM]$ as before. Left action by $g \in \mathcal{G}$ induces a natural column permutation $\sigma_c = I_{(m+1)k} \otimes \sigma_G \oplus I_{(m+1)(n-k)} \otimes \sigma_G$ where $\sigma_g(i) = j$ if $gg_i = g_j$. Furthermore, we note that both check matrices given in Theorem 4 contain $H_{\text{lower}} = I_{(m+1)k} \otimes H_1 \oplus I_{(m+1)(n-k)} \otimes P_H$ which commutes with σ_c . It suffice to augment checks that ensure the upper half is also preserved, yielding the $(m - 1)mk$ additional checks and $(m - 1)t$ contribution to column weight. \square

Similar to before, when we have more information about Σ (or the related \mathcal{G}), we can come up with sharper bounds:

Corollary B.5 (Conversion: Local CNOTs). *Let us be given a code $C(G, H)$ and let $(g, \sigma) \in \mathcal{A}(G)$ be an order-2 CNOT circuit on t bits where $g\sigma = G$. There exists a valid check matrix H' using t additional checks, and a row permutation $\rho \in P_{n+t}$, such that $\rho H'\sigma = H'$. Furthermore, if H is w bounded, H' is $w + t + 1$ -bounded.*

C CQLU Logical Operations

Given the matrix automorphism guarantees, as shown in [40], we can construct Hypergraph product and Homological product codes that inherits the code automorphisms as fault tolerant logical operations implementable via qubit relabeling. In this section, we focus on HGPS codes and study their matrix automorphism groups.

C.1 Dirty Shifts

First, let us construct the basis needed to realize the dirty cyclic shifts as matrix automorphisms.

Proposition C.1. Let P_i be the cyclic shift matrix on i elements. Given the binary simplex code \mathcal{S}_r with a circulant check matrix H_r . Then, P_{2^r-1} is a matrix automorphism, and exist a basis G for which the corresponding logical action of P_{2^r-1} is

$$g_{ds} = \begin{bmatrix} & & * & \\ 1 & & * & \\ & 1 & * & \\ & & \ddots & * \\ & & & 1 & * \end{bmatrix}, \quad (47)$$

which implements a cyclic row permutation of G plus a CNOT-fanout gate.

Proof. It is easy to see that the column shift matrix $P = P_{2^r-1}$ is indeed a matrix automorphism by definition of it being circulant. Suppose the logical action is g , we can also show that g has order $2^r - 1$, following from Fact 6 and since P has order $2^r - 1$.

Now, let $c \in \mathcal{S}_r$ be a non-zero codeword and define $B = \{c_i | c_i = c \cdot P^i, 0 \leq i < r\}$. Suppose B is a spanning set (for example, picking $c = [1, 1, \dots, 1, 0, 0, \dots, 0]$ works). Then, the generator matrix G_B built from stacking $v \in B$ as rows is the desired basis. Indeed, for each $i < r - 2$, $c_i P = c_{i+1}$; column permutation by P shifts rows of G_B by one. Furthermore, since $\langle B \rangle$ is r -dimensional and P is a code automorphism, $\langle B \rangle = \mathcal{S}_r$, and that $c_{r-1} P \in \mathcal{S}_r = \sum_{0 \leq i < r} b_i c_i$. Let g be the operator where $gB = BP$; it follows that

$$g_{ds} = \begin{bmatrix} & b_0 & & \\ 1 & b_1 & & \\ & \ddots & \vdots & \\ & & 1 & b_{r-1} \end{bmatrix}, \quad (48)$$

as desired. \square

C.2 autoCNOTs

For \mathcal{S}_4 , there exists non-trivial matrix automorphisms as well using H_4 given in Table 3 that can implement a order-2 logical circuit given a basis. Furthermore, by choosing different generator matrices, we can obtain a wide range of codes with various logical operators in the same conjugacy class.

Proposition C.2. Let τ_4 be the permutation matrix on 16 elements that performs a transposition on 4×4 square of the 16 elements in lexicographical order. That is, suppose $i = 4a + b$ for some $a, b < 4$, then $\tau(i = 4a + b) \mapsto j = 4b + a$. Let P_{auto} be the permutation obtained by removing the first element from τ_4 . Then, P_{auto} is a matrix automorphism for \mathcal{S}_4 with $H_4 = I + P_{15} + P_{15}^4$. Furthermore, there exist a basis G for which the corresponding logical action of P_{auto} is g iff g is conjugate

to $g_{SWAP} = I \otimes X$; that is, if there exists h such that:

$$hgh^{-1} = \begin{bmatrix} & 1 & & \\ & 1 & & \\ & & 1 & \\ & & & 1 \end{bmatrix}. \quad (49)$$

Note, by choosing $h' = \begin{bmatrix} 1 & & & \\ & 1 & & \\ 1 & & 1 & \\ & 1 & & 1 \end{bmatrix}$, we obtain $g_{auto} =$

$$\begin{bmatrix} 1 & & & \\ 1 & 1 & & \\ 1 & & 1 & \\ 1 & 1 & 1 & 1 \end{bmatrix} \text{ used in the main text.}$$

Proof. Note P_{auto} is an involution, and $P_{auto}P_{15}P_{auto} = P_{15}^4$; let each $i = 4a + b$ be represented by an ordered tuple (a, b) , we have $P_{auto}P_{15}P_{auto}(a, b) = P_{auto}P_{15}(b, a) = P_{auto}(b, a + 1) = (a + 1, b) = P_{15}^4(a, b)$. It follows that $H_4P_{auto} = H_4$.

To give a basis where the resulting logical action is a disjoint pair of SWAPs, we can find c_1, c_2 such that the basis $\{c_1, c_1P_{auto}, c_2, c_2P_{auto}\}$ is spanning. Let this generator matrix be G_{SWAP} . Then, for any invertible h , $G' = hG$ is also a valid generator matrix, and applying P_{auto} on G' gives g :

$$\begin{aligned} G'P_{auto} &= hG_{SWAP}P_{auto} = hg_{SWAP}G_{SWAP} = gG' \\ &\iff g = hg_{SWAP}h^{-1} \end{aligned}$$

which is conjugate to g_{SWAP} , as desired. \square

There are many choices that satisfy both propositions, giving us a code with desired ISAs.

While the primitive polynomial for \mathcal{S}_4 allows for a wide class of logical actions to be embedded, it is not guaranteed to be the case for larger r . Indeed, we find that the primitive polynomials as reported in Table 3 do not admit similar symmetries for any $r > 4$ via a numerical search, which means code modifications are unavoidable. However, beyond the check extensions already presented, there may exist circulant matrices with more terms that enforces the symmetry, but we leave this as future work to perform more intensive search.

C.3 Global Transversal Operations

In addition to automorphism gates, we briefly describe other transversal gates we can apply to the HGPS code. First, by virtue of the HGP construction, we can apply puncturing/augmenting techniques to \mathcal{S}_4 to achieve homomorphic CNOTs and homomorphic measurements between different code blocks, as done in [41]. By virtue of being a square symmetric code, the HGPS codes can access transversal H -SWAP gate, CZ-S gate, and sibling-CZs as give in [74]. These gates allow us to implement:

1. Hadamard on all logical qubits, plus a logical transpose,

2. S/S^\dagger gates on $2\sqrt{k}$ diagonal qubits, and CZ s on transpose-correspondent logical qubits in the same sector,
3. CZ gates between correspondent logical qubits in both sectors.

These operations allow us to produce and consume $|i\rangle$ state on the diagonal efficiently. For a more complete treatment, we refer readers to [41, 74].

D Circuit Compilations

In this section, we give the exact CQLU circuit implementation for quantum adder and related state preparation.

Figure 19 shows the full adder derivation:

- *Step 1:* we propagate the Pauli corrections arising from Bell-measurement through the circuit, possibly flipping the S -correction from $|T\rangle$ injections.
- *Step 2:* commuting the final CNOT in the MAJ block towards past the measurement bell. This creates an additional CNOT correction highlighted in blue.
- *Step 3-5:* commuting the S corrections past bell measurements.
- *Step 6a:* commuting the first CNOT in the MAJ (highlighted in green) past the fan-in, adding an additional CNOT correction (dashed-grey).
- *Step 6b* The newly added CNOT is then commuted past the bell-pair generation, leading to two CNOTs highlighted in blue, one of which acts trivially.
- *Step 7a:* adding two pairs of CNOTs and commuting them past the fanouts and T gates in the middle.
- *Step 7b:* the additional CNOT corrections cancel each other out.
- *Step 8-9:* finally, we conjugate by global H to change orientations of the CNOTs, and use a transversal SWAP to prepare the block for reactive measurements.

Figure 20 gives a spacial layout and exact CQLU operations required, alone with the state-prep step that can be done offline. This circuit has at most 4 active blocks in any time step.

Derivations for UMA and temporary AND-Toffoli (used in QROM) can be obtained following similar transformations, which we do not describe explicitly here. The QROM circuit used in [15] consist of temperoray-AND Toffolis and CNOT fanouts, which can be performed by consuming a GHZ state on n -qubits [67], which is included within Figure 20.

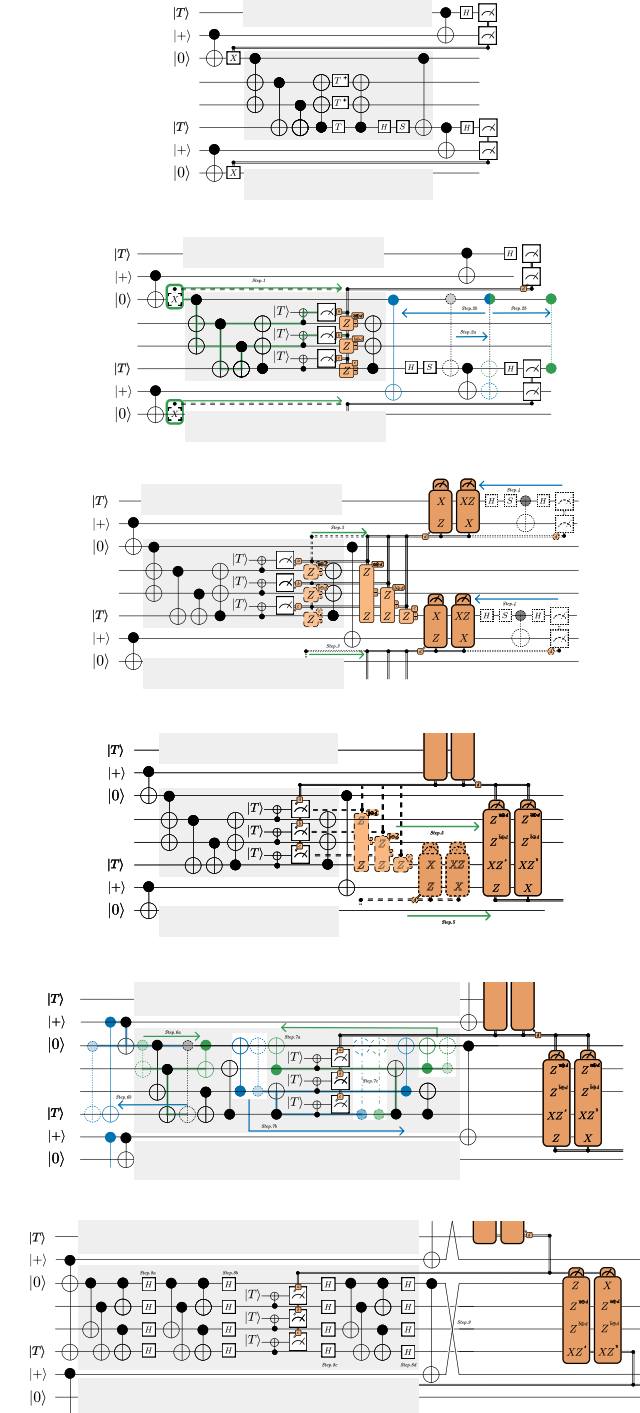


Figure 19. Full derivation of the MAJ blocks implemented using CQLU instructions. Pauli corrections that commutes with non-Clifford operations are tracked in software.

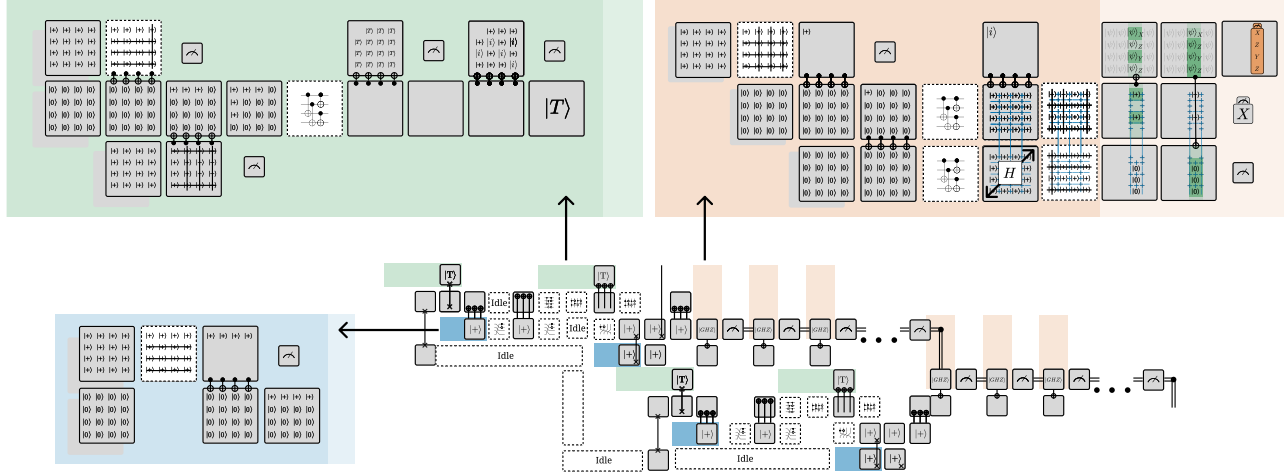


Figure 20. The exact compiled adder circuit, with offline state factories produced. Initial state preparation (blue) and T preparation (green) can be done completely offline. GHZ states for reactive measurements (orange) can be carried out mostly offline (dark orange), with two additional CNOTs and a measurement (light orange).